AFIT/GE/ENG/97D-10

A WIRE ANTENNA DESIGNED FOR SPACE WAVE RADIATION OVER THE EARTH

USING A GENETIC ALGORITHM

THESIS
Brian S. Sandlin
Captain, USAF

AFIT/GE/ENG/97D-10

19980128 099

The views expressed in this thesis are those of the author and do not reflect the official policy or position of the Department of Defense or the U. S. Government.

AFIT/GE/ENG/97D-10

A WIRE ANTENNA DESIGNED FOR SPACE WAVE RADIATION OVER

THE EARTH USING A GENETIC ALGORITHM

THESIS

Presented to the Faculty of the School of Engineering

of the Air Force Institute of Technology

Air University

In Partial Fulfillment of the

Requirements for the Degree of

Master of Science in Electrical Engineering

Brian S. Sandlin, B.S.E.E.
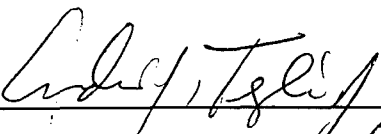
Captain, USAF

December, 1997

A WIRE ANTENNA DESIGNED FOR SPACE WAVE RADIATION OVER THE EARTH USING A GENETIC ALGORITHM

Brian S. Sandlin, B.S.E.E.

Captain, USAF

Approved:

_____   _____
Andrew J. Terzuoli, Ph.D., Committee Chairman   Date

Department of Electrical and Computer Engineering

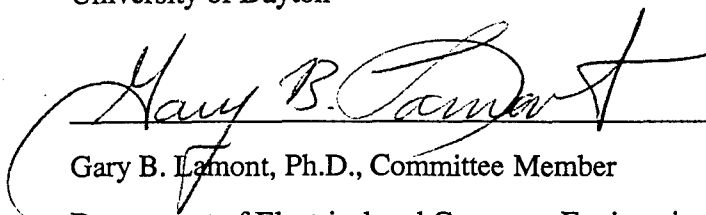_____   _____
Gary A. Thiele, Ph.D., Committee Member   Date

Department of Electrical and Computer Engineering

University of Dayton

_____   _____
Gary B. Lamont, Ph.D., Committee Member   Date

Department of Electrical and Computer Engineering

_____   _____
Peter J. Collins, Ph.D., Major, Committee Member   Date

Department of Electrical and Computer Engineering

Acknowledgements

Bug,

You are my sunshine . . .

Table of Contents

List of Figures

List of Tables

AFIT/GE/ENG/97D-10

Abstract

A wire antenna is designed for optimal performance at low elevation angles in the presence of a lossy half-space. A simple genetic algorithm (GA) and GENOCOP III software are each integrated with Numerical Electromagnetics Code Version 4.1 (NEC4.1) to optimize a wire antenna geometry for multiple objectives: power gain, azimuthal symmetry, and input impedance. The performance of the two versions of the integrated GA are compared. Several of the resulting antennas are analyzed, and an antenna is proposed for use in a Remote Intrusion Monitoring System (RIMS). Simulations suggest that the proposed antenna, which is well-matched, offers a significant increase in power gain at low elevation angles compared to the quarter-wavelength monopole. The performance of the proposed antenna surpasses that of the monopole at the necessary frequencies and a wide range of soil types. Also, the new antenna performance is not degraded by structure geometry perturbations.

A WIRE ANTENNA DESIGNED FOR SPACE WAVE RADIATION OVER THE EARTH USING A GENETIC ALGORITHM

I. Introduction

1.1   Background

In this modern age antennas are a vital component in a multitude of communication systems like broadcast radio, television, cellular phones, pagers, citizens-band radio, and Hamm radio, which all rely on an antenna to effectively and efficiently radiate power. Often, the designer's choice of an antenna is based upon presuppositions and familiarity with classical antenna designs.

One example of a classical design is the monopole antenna, particularly the vertical monopole. Vertical monopole antennas are used on buildings and towers, with our cordless and cellular phones, cars, and portable radios. Why is the vertical monopole so common? Not only are they inexpensive, lightweight, and reliable, but they provide acceptable and *predictable* performance for a broad range of applications.

In the past, antenna design was a process which was mostly intuitive in nature, based upon the designer's knowledge of the electromagetic capabilities of different structures, materials, and loading mechanisms. The engineer develops the theory for the antenna, formulating the currents on the antenna to be placed in the radiation integral, and the radiation capabilities are deduced. By varying certain parameters in the antenna, design equations are developed to optimize many characteristics: directivity, gain, efficiency, impedance, etc.

The classical design process holds true for the vertical monopole, also. These antennas are supplemented with a variety of loading structures, be they geometric (e.g. multiple turns) or circuit-based. Common designs also incorporate a number of other additions such as dielectric sheaths and radial wire ground screens. All such additions have been investigated

and optimized for particular applications. Despite the variety of modifications, the basic premise remains the same ... a vertical monopole.

1.2 Remote Intrusion Monitoring System (RIMS)

The traditional and most noticible application of the vertical monopole is within the context of personal communications systems, but the monopole's use is certainly not restricted to this arena. In particular, another type of system which uses the vertical monopole falls into the broader class of *remote sensing* systems. The system of interest is called a Remote Intrusion Monitoring System (RIMS). In general, a RIMS is a system used to observe activity within a distant region. Application of a RIMS extends well beyond the monitoring and enforcement of security implied by the name because a RIMS can also be used for gathering telemetry in the region of interest (e.g. to collect data about the seismic activity in the proximity of a volcano).

1.2.1 Description. A number of integrated components accomplish the challenging task of remote sensing taken on by a RIMS. In general, a RIMS contains some or all of the components shown in Figure 1.1. A general understanding of the system description is beneficial to understanding the design constraints in Section 1.2.2 and evaluating the design approach.

- **Unattended Sensors** These units are physically located in the region of interest and are frequently buried, leaving only their antennas above ground. In situations and environments where sensors cannot be buried, they can be disguised in a like manner and to an appropriate extent, depending upon the application. Sensors are versatile because they can be customized to respond to different types of stimuli to include magnetic, seismic, passive infrared, or acoustic events.
- **Optical Sensor** This unit is strikingly similar in purpose to the unattended sensors with two exceptions: 1) the optical sensor provides visual information (with the same goal as the type of monitoring system found in banks, stores, etc.), and 2) since visual information is required, an additional camera unit must be attached via a closed circuit link as shown in Figure 1.1.
- **Field Processor** As the name implies, this component is positioned in the same environment as the sensors. The physical dimensions of this unit are larger than those of the sensors, so many of the operational requirements applicable to the sensors also apply to the field processor with the exception of functional capability, which is to receive the information—sent via the radio frequency (RF) link—from the multitude of sensors
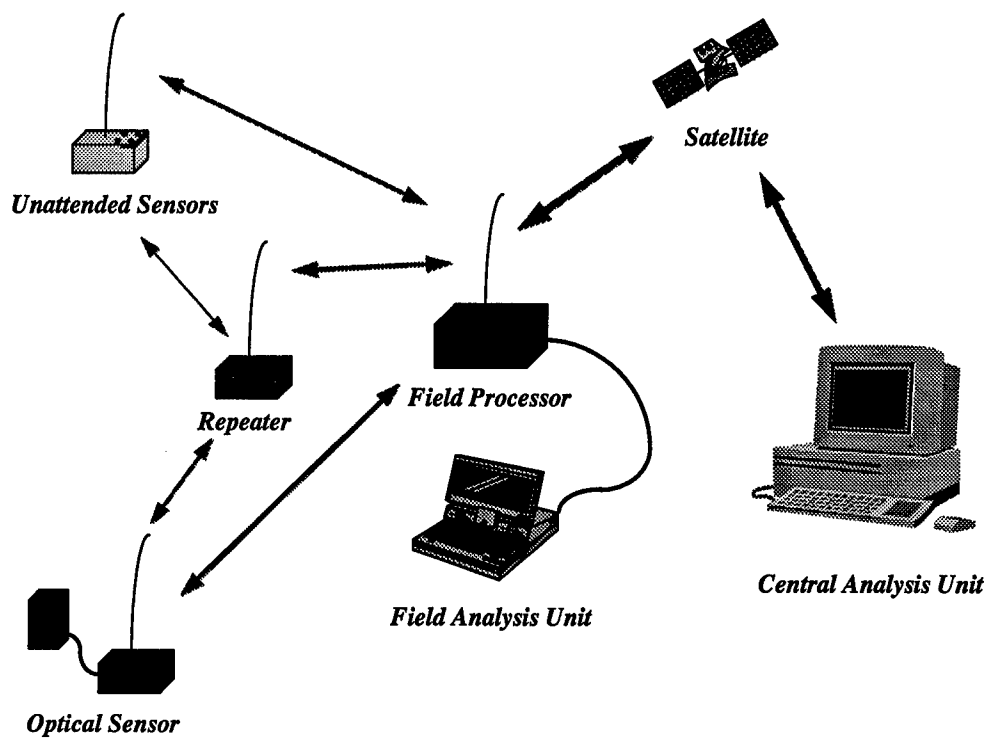
Figure 1.1   Common Components of a RIMS

and format the data as input to display and analysis software located in the field and central analysis units.

- **Field Analysis Unit** This is an optional unit and is essentially a laptop personal computer that can be connected directly to the field processor. The presence of this unit in no way effects the job performed by the field processor because it is simply a medium for interpreting the raw sensor data using data analysis software.

- **Central Analysis Unit** Eventually, all of the sensor information arrives (via satellite) at the central analysis unit, on which is also resident the data analysis software used by the field analysis unit.

- **Repeater** This unit receives and retransmits signals from the sensors. Theoretically, repeaters allow for greater distances between the other components. The reality is that repeaters in some operational systems are not adequate.

In a typical RIMS the unattended sensors, optical sensors, repeaters, and field processors all use vertical monopole antennas constructed of very thin wires. A first-look analysis indicates that these antennas are designed using traditional methods without much consideration for the environment surrounding the operational antenna. A desirable radiation pattern for this type of application is that of a vertical dipole radiating in free space, since its radiation pattern is azimuthally symmetric and the input impedance is perfectly matched when the length of the dipole is half that of the wavelength (λ) of the signal exciting the dipole. For this reason, the RIMS monopole antenna is $\lambda/4$ in length. The apparent assumption in this design is that if the ground can be approximated as a perfect conductor, then image theory applies, and the result is equivalent to the $\lambda/2$ dipole in free space.

The reality is startling, at least for the RIMS user. The earth is far from acting like a perfect conductor, and image theory breaks down in the far-field radiation pattern. A perfectly conducting ground has an infinite electrical conductivity (σ), but the truth is that the conductivities of many types of earth soil are far from infinite as observed in Table 1.1 (1:67). The result is a severely attenuated field at low elevation angles which drastically impacts the RIMS user who desires system components to be located on the ground.

1.2.2 Design Constraints. The most common application of a RIMS is to perform covert monitoring. In general, the field processor, sensors, and optical sensor are located in a non-supportive environment. This application has two broad implications. The first is that the user cannot—or at least not be guaranteed—access to the system. The second is that the

1-4

SURFACE TYPE	$\sigma\ (\frac{m\mho}{m})$
Marsh Land	111
Desert Land	11
Dry Soil	10
Good Jungle	30
Average Land	27.8
Medium Jungle	10
Rich, Damp Soil	15
Very Dry Soil	1
Rocky Ground	1
Thin Soil over Rock	1.5
Poor Jungle	2
Tundra	0.4
Dry, Sandy Soil	1
Fresh Water	5
Arctic Ice	0.025
Glacier Ice	0.04

Table 1.1 **Typical Values of Conductivity, σ, in millimhos/meter ($m\mho$/m) for Different Types of Earth Surface**

design must blend into the environment without being noticed. These major factors drive a number of other considerations.

- In physical terms, any antenna design should not be large or bulky. For meeting this requirement, current RIMS implementations that incorporate the thin-wire monopole are excellent.

- The sensors and field processor are often located in foliage. An electromagnetic wave's ability to penetrate foliage is inversely proportional to frequency (2:1198-1206), leading to an important design trade-off. Larger antennas are required for successful communications at lower frequencies. The average RIMS compromises by using the very high frequency (VHF) band.

- The amount of power used by the sensors for transmitting a message to the field processor must be sufficient, but the size of the power supply cannot force the physical dimensions of the sensors to unreasonable levels.

- The voltage source driving the antenna should be located very close to or on the ground. Feeding the antenna with a bulky transmission line or positioning the antenna on a coaxial mast *cannot* be done.

- The antenna should radiate uniformly in the azimuth direction. Because the non-supporting environment places time restrictions upon the positioning of components during RIMS installation, the antenna orientation cannot be guaranteed.

- For the remote components (e.g. sensors), little or no opportunity for maintenance exists, so they are often considered expendable. Therefore, the design should incorporate dependability and a zero-maintenance requirement, as well as reasonable cost.

1.3   Research Problem

The impact of the earth upon the fields and power radiated by near-ground antennas has been extensively studied in both emperical and theoretical domains. Understood to a lesser extent is the impact of antenna geometry upon the power radiated at low elevation angles. No effort has been made to optimize the antenna geometry given the real-earth consideration.

A wire-antenna design is clearly desirable for the type of context associated with a RIMS, but because of the problem complexity combined with the design constraints, a classical design approach is impractical. A stochastic search method, the genetic algorithm (GA), not only makes a solution attainable, it finds a solution that performs better than thought possible.

Thus, the research problem is simple: to use a GA to optimize a wire antenna geometry in the presence of a less-than-perfectly-conducting half-space for the objectives of power gain, symmetry of radiated power in azimuth, and matched input impedence. The reason for the first two objectives is obvious given the design context and the performance of existing designs. Meeting the last objective, that of matching the impedence will allow maximum power transfer, a topic reminiscent of a basic circuits course.

1.4   Terminology

Since this research is a hybrid of two worlds, electromagnetics and genetic algorithms, the explanation of terminology in each world is useful.

Using a physics definition, the term *ground plane* refers to a region of zero electrical potential. Often in literature, the term ground plane refers to a part of an antenna otherwise termed the *ground mechanism*, *ground screen* or *ground structure*. Ground plane is also commonly used to talk about a half-space such as the earth, but this research will keep the terminology separate. When the term *ground* is used alone, it will refer to the earth. The term *lossy* describes a medium with a finite σ, so that attenuation occurs as waves propagate through it.

In the GA domain, *features* are the free parameters in the design, upon which the optimization occurs (3:21-22). The range of values or the discrete values that the feature can possess is called the *feature value* (3:21-22). Features and feature values are synonymous with the biological genetic terminology *genes* and *alleles* (3:21-22). The *string* corresponds to a biological *chromosome* and is a collection of features. In the GA introduced in this research, each string represents a complete structure, or antenna design, which corresponds to the *genotype* in biology (3:21-22). The *fitness* is a single value associated with each string, according to its capabilities. In the case of this research, fitness is a combination of the objectives mentioned in Section 1.3. The biological counterpart is the *phenotype* (3:21-22). The *population* is the collection of strings that will be maintained during the execution of the genetic algorithm. *Crossover* is the function of generating new strings, *offspring*, based on the feature values of existing strings. *Selection* is the process by which strings are chosen for crossover. A *generation* is a snapshot of the population at distinct periods in the execution of the algorithm. The concept of generations is really only useful as applied to simple GAs. The complex GA used in this research, GENOCOP III, has no real sense of generation.

1.5 Related Research

For some time, genetic algorithms have been applied to electromagnetics-related problems. Much research has occurred in the area of array design, as GAs have been used to optimize arrays and absorbers.

More specifically-related research was conducted by Altshuler and Linden (4:74,76). They designed what they called a *crooked-wire antenna* with an elementary GA for the purpose of developing circular polarization for hemispherical coverage to be applied to satellite communications. Despite some similarity with their research, this effort is a significant departure from their work in the following areas:

- The ground plane on which the antenna sits is not perfectly conducting, it is composed of a lossy material with some permittivity, ϵ, not equal to that of free space.
- Multi-objective optimization with a weighted sum approach is implemented to synthesize the antenna for the objectives described in Section 1.3.

- The configuration of the simple GA used to develop the antenna is not chosen at random but is chosen as the best of a pool of different configurations.

- The results of the simple GA are directly compared with those generated by a sophisticated GA software package.

- The constraints on the geometry are extended beyond that of connecting the wires in series.

1.6 Assumptions

1.6.1 Smooth Earth. It was not prudent for the research to account for an earth surface with realistic terrain because of the variety of possible terrains that would be encountered by the RIMS. For antenna design purposes, it was sufficient to allow an earth with a smooth surface. The path loss associated with a variety of terrain types has been widely studied and is reasonably well understood (5:6-21).

1.6.2 Earth Curvature Ignored. The earth is assumed to be flat. Curvature is ignored since the range between typical RIMS components which use the $\lambda/4$ monopole is well within VHF line-of-sight, which refers to the maximum distance between a VHF transmitter and receiver. Because of the earth's curvature and the refractive and diffractive characteristics of RF waves in the atmosphere, this distance depends on the height of the transmitter, the height of the receiver, and the wavelength (6:553–558). This assumption works well with the NEC4.1 code used for calculations, since the code defaults to a flat earth.

1.6.3 Multipath Ignored. The environment surrounding the RIMS is not only flat but extends well beyond the perimeter of the system. By making this assumption, multipath effects are ignored. In reality, multipath is a significant factor in a operational RF system, and is the focus of a significant amount of research, particularly in the area of mobile communications (7:201).

1.6.4 Earth Parameters Constant. For the region immediately surrounding and encompassed by the system, the approximation is made that the electrical parameters of the earth, particularly the relative permittivity (dielectric constant), ϵ_r, and the conductivity, σ,

are constant and do not vary within or around the region of interest. This constraint says that, in effect, the earth is homogenous in the region of interest, a condition that is highly unlikely given the real earth, but it is an approximation that is necessary to constrain the problem accordingly. To overcome this assumption, the interaction of the best antenna design with different types of earth is researched.

   1.6.5   Circuit Ground.   In many RIMS, the ground for the signal generation circuitry is not directly connected to the ground but to a circuit board ground. In these cases, the ground for the circuit components is a ground strip or a metal sheet manufactured in the layers of the circuit board. No grounding rod is used to connect the circuit board ground to real ground. The difference in electrical potential between the circuit board ground and the real earth is not modeled in this research. Instead, the assumption is that the earth and circuit grounds are connected in some manner.

1.7   Scope

   The research proposes a system antenna design, taking into account the link budget. The proposed antenna will be directly compared to the $\lambda/4$ monopole currently used in RIMS applications.

   The antenna will be designed for the center frequency of the band of interest. Since the capabilities of existing RIMS matching networks are unknown, any matching network considerations will be excluded from the models.

1.8   Approach

   The first step in the approach to solving the research problem was to develop GAs which interface with the moment method code (MoM), Numerical Electromagnetics Code Version 4.1 (NEC4.1), to develop a wire antenna geometry. The wire endpoints become the features that the GAs search to find the optimal design. The fitness is determined by a weighted sum of multiple objectives.

The next step is to compare the resulting antenna design found by the simple version of the integrated GA with one found by the integration of NEC4.1 and the more sophisticated GA software package, GENOCOP III, using a simple geometry definition. Then, the most suitable configuration of the SGA is found and applied to two other geometry definitions.

The third step is to develop the method by which the resulting genetically-designed antennas are to be evaluated. Not only will the gain be investigated, but symmetry, input impedance, and a link budget analysis are performed.

1.9 Materials

Gerald Burke and Lawrence Livermore National Laboratory (LLNL) made available the NEC4.1 software. This code is used in two ways: 1) to evaluate possible antenna designs within the structure of a GA for the purpose of geometry optimization, and 2) to provide necessary analysis of optimized designs.

A simple GA (SGA) is written in Fortran 77, based on the knowledge obtained from research. This SGA is integrated with NEC4.1 to form the first of two *integrated* wire-antenna optimization algorithms. With the assistance of two Air Force Institute of Technology (AFIT) Ph.D. students, Dave Van Veldhuizen and Robert Marmelstein, the second of the two integrated wire-antenna optimization algorithms was created using the GENOCOP III software package. This routine is named the GENOCOP III-GA (GGA).

1.10 Goals

The purpose of the research is to conduct a thorough design approach taking into account all aspects of antenna design, to include the following goals:

- Gain a reasonable understanding of genetic algorithms and apply knowledge to problem.

- Directly compare results of the SGA to those of a more sophisticated design to gain further understanding of evolutionary algorithms. Point out any deficiencies between simple algorithms and complex GAs, keeping in mind the outcome analysis.

- Design an antenna that accounts for all aspects of the design context, one that can actually be built and placed in operational use.

- Propose a design with input impedance frequency characteristics that are reasonable for matching across the entire band.

II. Literature Review

2.1 Antennas Near the Lossy Earth

The general problem of a dipole near the lossy earth is well understood. Sommerfeld first explored this problem in 1909 by investigating the effects of a flat earth on a vertical electric dipole, theorizing the concept of a *ground wave* that propagates through the earth's skin, which acts much like a wave guide (8:665–736). Since the early research of Sommerfeld, many others have contributed to the knowledge base in this area.

Because the ground wave propagates through a lossy medium, it experiences attenuation. In 1936, Norton redeveloped the ground attenuation function first given by Sommerfeld, simplifying the equations derived by Sommerfeld into more interpretable and useful forms (9:1368–1373). The next year, Norton dissected the vertical-dipole-near-earth problem further by discussing the *wave tilt* phenomena of the trapped surface wave (10:1197). The ground wave is elliptically polarized, and the elliptical characteristics of axial ratio and tilt angle are dependant upon the frequency and the ground parameters (10:1197). Norton also looked at the Poynting vector and showed how it is directed toward the ground, causing energy absorption by the ground (11:1230–1232).

Later, Norton derived approximate general formulas of the electric field for a vertical and horizontal electric dipole in the presence of the lossy half-space, accurate for the first-order space wave and the second-order ground wave (11:1206–1207,1232). He also derived similar expressions for a loop (11:1208–1209). However, Norton made no conclusions about the relative worth of each antenna in terms of gain observed at low elevation angles.

Many years later, Jordan and Balmain simplified the Norton expressions further by removing the higher-order $1/R$ terms, effectively taking the expression into the far field (12:639). The simplified expression for the vertical electric field component of a vertical electric dipole radiating in the presence of earth is then given as

$$E_Z^v = j30\beta I\, dl \left[\cos^2\psi \left(\frac{e^{-j\beta R_1}}{R_1} + R_v \frac{e^{-j\beta R_2}}{R_2} \right) \right.$$
$$\left. + (1 - R_v)\left(1 - u^2 + u^4 \cos^2\psi\right) F \frac{e^{-j\beta R_2}}{R_2} \right] \quad , \tag{2.1}$$

where

$$u^2 = \frac{1}{\epsilon_r - j\frac{\sigma}{\omega\epsilon_o}} \quad , \tag{2.2}$$

$$F = 1 - j\sqrt{\pi\xi}\, e^{-\xi}\mathrm{erfc}\left(j\sqrt{\xi}\right) \quad , \tag{2.3}$$

$$\xi = \frac{-j\beta R_1 u^2 \left(1 - u^2 \cos^2\psi\right)}{2} \left[1 - \frac{\sin\psi}{u\sqrt{1 - u^2 \cos^2\psi}}\right]^2 \quad , \tag{2.4}$$

and

$$\mathrm{erfc}(j\sqrt{\xi}) = \frac{2}{\sqrt{\xi}} \int_{j\sqrt{\xi}}^{\infty} e^{-v^2}\, dv \quad , \tag{2.5}$$

with the propagation constant (β), current magnitude (I), differential length of the vertical dipole (dl), elevation angle (ψ), distance from the dipole (R_1), distance from the image (R_2), vertical polarization reflection coefficient (R_v), permittivity of free space (ϵ_o), relative permittivity of the earth (ϵ_r), and the conductivity of the earth (σ) are all known values. The function F is defined as the ground wave attenuation function (12:639).

Looking at the two equations, the field can be divided into two terms, the *space wave* and the *surface wave* (often called the *lateral wave* in the literature) (12:639). The surface wave is the combination of a direct wave and a reflected wave and is described in the $1/R_1$ and $1/R_2$ terms (12:639). The surface wave is distinguished as the term containing F (12:639).

Insight into the ground wave term is gained by looking at the attentuation function, F. Letting $A = |F|$ be the ground wave attenuation factor and looking only at the propagation along the surface, $\psi = 0$, Equation 2.4 reduces to

$$\xi = \frac{-j\beta R_1 u^2 \left(1 - u^2\right)}{2} = p e^{jb} \quad , \tag{2.6}$$

where p is described as the *numerical distance* and b is the *phase constant* (12:646). In their text, Jordan and Balmain give approximate values for p and b at $\psi = 0$ (12:646):

$$p \cong \frac{\pi R \xi \epsilon_o}{\lambda \sigma} \cos b \qquad (2.7)$$

and

$$b \cong \arctan \left(\frac{(\epsilon_r + 1) \xi \epsilon_o}{\sigma} \right) \ . \qquad (2.8)$$

From Equations 2.7 and 2.8, one can show that the numerical distance is proportional to the square of the frequency and the distance from the source and is inversely proportional to the conductivity of the earth (12:646). Therefore, for any value of b, A very quickly becomes small as p gets increasingly larger (12:646). The key result is that the magnitude of the ground wave is very small at large distances from the antenna, high frequencies and near poorly conducting earth (12:646).

To reduce the losses in the ground, a number of antenna configurations have been proposed over the years, most of them focusing on the use of a monopole antenna over some form of solid or mesh ground mechanism. Wait investigated a sinusoidally-driven monopole on a ground screen and concluded that the presence of the screen impacted the input impedance far more than it improved the far-field radiation pattern (13:181). Collin and Zucker reiterated this result by pointing out that the size of the ground system—be it radial wires, a mesh of wires, or a solid disk—must be large compared to wavelength in order for it to improve the patterns (14:435).

It is common knowledge that in the presence of ground the dipole is a better antenna than the monopole (15:64). Adding a ground mechnism to a monopole is an attempt to approximate the dipole, so the better the ground screen, the better the approximation (15:64). Ramsay proposed the several configurations shown in Figure 2.1 as attempts to approximate the dipole with different linear antennas and ground screen combinations, which could be composed of solid material or meshed wires (15:69–70).
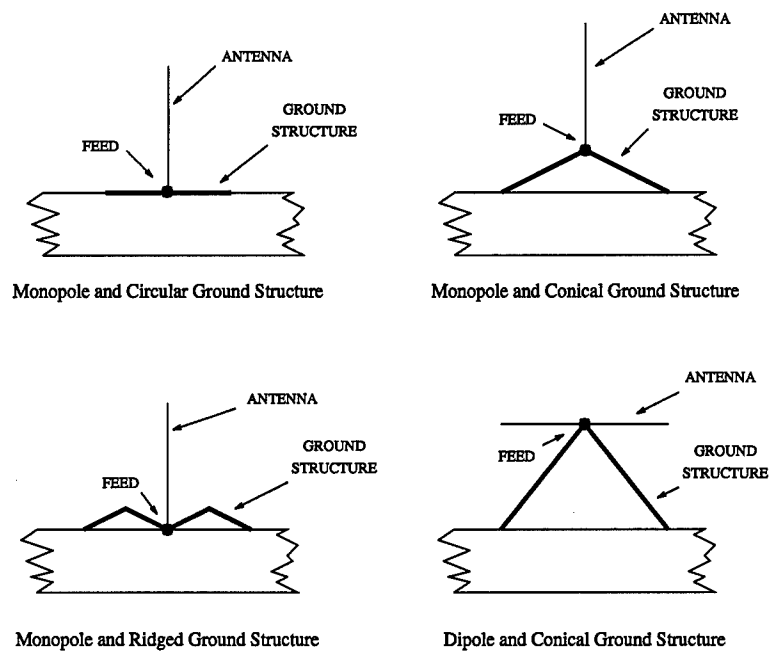
Figure 2.1   **Antenna and Ground Structure Combinations Proposed by Ramsay to Reduce Ground Losses.**

For frequencies in the high frequency (HF) band, antenna designers have focused on optimizing the ground wave. In particular, Thomas and Haack developed the *dart antenna* specifically for frequencies from 8–26 MHz, which is closely approximated by a dipole radiating in free space (16:298). Trainotti proposed an asymmetrical dipole antenna that uses its guy wires as radiating elements to produce a ground wave and achieves good results at a frequency of 30 MHz (17:106).

King points out that the space wave term is attenutated by a $1/R$ term while the ground wave is modified by a $1/R^2$ term (18:386). He also adds that the ground wave is only a significant contributor to the near field for highly-conducting ground, and that the ground-wave contribution to the far-field is insignificant for most all types of ground (18:386). To capitalize on the ground wave at VHF frequencies, two requirements exist. The first is that the amount of transmission power must be great, and the second is that observation distance must be small (19:20). The theory behind these requirements is supported with measured data (19:22).

On the more practical side, amateur radio enthusiasts have dealt with the issue of wave attenuation due to the lossy earth for some time. For those interested in a ground-based antenna, amateur radio experts suggest the use of a $5\lambda/8$ monopole because of its advantages in low-elevation gain and its omnidirectional (in azimuth) radiation pattern (20:136). Because the main portion of the current distribution on this antenna is lifted off the ground, the $5\lambda/8$ monopole is described as having the lowest angle of radiation and the highest gain when compared to other monopoles (21:177). The disadvantage of the $5\lambda/8$ monopole antenna is its input impedance, which is commonly overcome by amateur radio antenna designers by stub matching (21:193). This research seeks to design a perfectly matched antenna, thereby eliminating the need for stub matching.

2.2 Genetic Algorithms Applied to Electromagnetics Problems

Modern research is beginning to uncover a plethora of applications for the genetic algorithm, particularly in the field of electromagnetic research. Problems from multi-layer

absorber design to antenna design have greatly benefited from the ability of the GA to optimize large parameter sets.

For those unfamiliar with the principles behind GAs, a good introduction is provided by Haupt (22:7-9). In his article, Haupt covers the basic terminology and provides a flowchart for a simple genetic algorithm. Haupt's terminology is slanted toward the counterpart biological terminology given in Section 1.4. His explanation of terms and examples are tailored for binary-coded features, but the same principles can be applied to real-coded values. Haupt even goes so far as to provide the MATLAB code for a simple genetic algorithm (22:9).

Haupt provides three examples of electromagnetic applications for genetic algorithms. The first example is to optimize radar cross section (RCS) backscatter from a one-dimensional, symmetric, thinned grid of perfectly conducting strips (22:10-11). In this example, the widths and spacing of the strips are kept constant, so the coded parameters indicate the existence of a strip within the grid (22:10). The fitness function seeks to minimize the maximum relative sidelobe level of the return. With an initial population of 80 strings, the GA was allowed to iterate through eight generations and was able to reduce the maximum sidelobe level from -13.3 dB (for the uniform grid) to -17.1 dB (22:10) . Haupt admits that the solution found by the GA may not be a global minimum, so he ran the GA multiple times and was not able to produce better results, even with larger numbers of chromosomes and an increased mutation rate (22:11).

Haupt's second example seeks to minimize the maximum sidelobe level of a 48-element array by controlling the element spacings. The uniform array with an inter-element spacing of $\lambda/2$ had a maximum sidelobe level of -13.26 dB (22:12). Haupt's GA finds a spacing that produces a maximum sidelobe level of -27.2 dB (22:12). For comparison sake, optimization of the 48-element array using the quasi-Newton algorithm produced a maximum sidelobe level of -21.2 dB (22:12). The GA didn't always outperform the quasi-Newton method, though. Haupt found that the quasi-Newton method found better solutions for arrays of eight elements or less (22:12). It appears that when the number of parameters in the problem increases the quasi-Newton method becomes trapped in local minima, but the GA does not (22:12).

The final example used by Haupt is that of minimizing the maximum-backscatter relative-sidlobe level of a resistively loaded perfectly conducting strip (22:12-13). The strip is 6λ wide and the widths and resistive values are optimized for the eight loads placed on each side of the strip (22:12). The performance of the GA compared to the quasi-Newton method was similar to that of the Haupt's second example because the GA was outperformed by the quasi-Newton algorithm only for problem definitions of ten loads or less (22:13).

Haupt outlines a number of considerations when using genetic algorithms. For instance, the intial population size is important because the solution space must be sampled appropriately (22:14). Haupt uses the general rule of thumb of using a population size that is 10 times the number of bits used to represent a string (22:14). In generating the random list for the intial population, Haupt uses a normal distribution for the array examples in the paper, which causes the center of the arrays to be more dense (22:14). With regard to selection, Haupt tried a number of methods including random, best with worst, and elitist, and he determined that the method that works best was elitist (22:14). For mutations, Haupt only mutates 1% of the strings with the stipulation that the best performing strings are not mutated (22:14).

Some final advise given by Haupt is with regard to algorithm convergence. With convergence criteria difficult to define, Haupt lets his GA iterate for 20 to 50 generations (22:14). He notes that for separate runs the GA doesn't necessarily converge to an identical solution (22:14). For instances where convergence is a problem, he suggests three possible approaches: increasing population size, increasing mutation rate, and constraining the problem (22:14).

Simple GAs are used quite frequently in electromagnetics research, and in many cases the GAs are tasked to maximize or minimize a single objective. Using an algorithm structure very similar to the one given by Haupt (22:7-9), Himdi developed a slot coupled loaded patch antenna which was optimized solely for input impedance (23:1702). Another example is that an absorber design may only seek to minimize the reflection coefficient over a range of incident wave angles (24:1709). In array design, Ares chose only to optimize the dynamic range of the array (25:1684).

A number of more sophisticated GA approaches have been investigated in the electromagnetic community. A four-iris rectangular waveguide filter was optimized by Weile and Michielssen using an extension of the basic GA, one that incorporated the *community string* concept, which greatly accelerated convergence (26:1669). Using the genetic algorithm software PGAPACK, Zuffada's research uncovered a never-before-demonstrated three-material-waveguide-grating transmission filter with a 0.007% bandwidth at the center frequency (27:1679). By implementing a *penalty function* in the determination of fitness, Marcano found improved results over the simple GA for optimizing linear and planar arrays (28:1690).

Several antennas have been optimized using the GA. For both kite and monopole wire antennas to be used in military applications, Mittra used a GA to optimize the parallel RLC circuit loads for their resistance, inductance, and capacitive values, as well as their location (29:1672).

In terms of optimizing geometries, Johnson and Rahmat-Samii employed a simple GA using both elitist and roulette-wheel selection and a 2.0% mutation rate to optimize a patch antenna (30:1665). In their approach, they chose to minimize the reflection coefficient at three frequencies (30:1665). The resulting geometry had a surprising, non-intuitive shape which not only met their requirements but was reasonable in terms of actually constructing the antenna (30:1666).

In the world of wire antenna design, Alshuler and Linden were the first to incorporate a GA for the purpose of manipulating a wire antenna geometry in an optimization problem. Their early research sought to optimize the monopole antenna loaded with a modified folded dipole of earlier research (31:871–876) for the precise geometrical lengths of the antenna (32:1–4).

From reading about the research performed by Altshuler and Linden, one can conclude that they developed their GA from scratch. One of the goals of this research is to point out the possible dangers of this approach. However, the simple type of GA is worthy of mention.

GA Characteristic	Method Used
Parameter Representation	Binary
Population Size	150
% Steady-State	50
Crossover	Single Point
Mutation Rate	0.0-0.9%
Selection	Weighted Roulette Wheel

Table 2.1   A Summary of Characteristics for the GA Used by Altshuler and Linden to Optimize the Geometry of the Monopole Loaded with a Modified Folded Dipole.

The building block of Altshuler and Linden's GA was their choice of binary parameter representation (32:2). Each of the wire length parameters in the loaded monopole were represented by five-bits and expressed in terms of wavelength (32:2). The number of bits was intentionally chosen with manufacturing tolerances in mind (32:2). With six parameters to optimize, each chromosome was represented by a 30-bit stream (32:2). Altshuler and Linden chose to maintain a population of 150 chromosomes, although the article makes no mention of why this number is chosen (32:2). They used a *steady-state* approach, keeping 50% of the population from generation to generation. The method of parent selection used was a *roulette wheel* (32:2). For crossover, they implemented a single-point binary crossover to create offspring (32:2). Table 2.1 summarizes the characteristics of the GA used by Altshuler and Linden.

Further research was performed by Altshuler and Linden to synthesize a wire antenna with properties of hemispherical coverage and circular polarization (4:74). For this problem, an antenna geometry consisting of five to eight series-connected wires is optimized for the same objectives as the monopole loaded with a modified folded dipole (4:78). First, the wires are confined to reside in a cube of dimension 0.5λ above a perfectly conducting ground plane (4:78). The beginning and end points of each wire in the antenna are coded as features, the strings being the collection of wires that form an antenna (4:78). Again, the fitness of each chromosome was determined by a single objective function. Gain is averaged over a range of zenith angles ($\theta=0-80°$) and azimuth angles ($\phi=0-360°$), both intervals being divided into 5°

increments, to produce G_{ave} (4:78). Then, the sum of the squared error from all the points is calculated using

$$fitness = \sum_{\phi,\theta} (G(\theta,\phi) - G_{ave})^2 \quad, \tag{2.9}$$

where $G(\theta,\phi)$ is the gain at a particular location (4:78). Although they claim to have optimized the antenna for RCP, they give no indication that they considered polarization in determining the fitness.

In later work, Altshuler and Linden attempted to tackle multi-objective optimization by adding a constant with a value dependent on the voltage standing wave ratio (VSWR) (33:1681). Their fitness computation becomes

$$fitness = \sum_{\phi,\theta} (G(\theta,\phi) - G_{ave})^2 + C \quad, \tag{2.10}$$

with

$$C = \begin{cases} 0.1 & \text{VSWR} < 3.0 \\ 1.0 & \text{VSWR} \geq 3.0 \end{cases} \tag{2.11}$$

One problem that occurs when using a binary form of this multi-objective optimization is evident when considering two designs of equal gain deviation (the sum term in Equation 2.10). Regardless of one such design having a VSWR much greater than 3.0 and the other having a VSWR only slightly greater than 3.0, both designs will have identical fitness scores. This method severely inhibits the ability of a GA to evolve toward desired fitness scores, since information is lost in the binary-handling of the VSWR objective.

Linden and Altshuler have investigated the use of a number of other techniques for the same problem. The results are shown in Table 2.2. Their investigation shows that the GA is an extremely effiecient method when compared to the techniques of random search or the stochastic hillclimber (4:80). The results obtained by Altshuler and Linden in Table 2.2 provided motivation to use GAs to develop an antenna for the RIMS application.

Search Method	# of Fitness Evaluation Required
Random Search	6.3×10^{14}
Stochastic Hillclimber	26,000
Genetic Algorithm	9000

Table 2.2   **Linden and Altshuler's Computation of the total Number of Fitness Computations Required to Achieve a Desired Fitness Score Under 500**

2.3   Research Opportunity

Given that the lossy earth boundary poses an intimidating physical restriction for antennas used in its presence and the complexity of the equations required for analyzing even the simplest of antennas given the earth condition, the opportunity presents itself to design an antenna for radiation over the earth. With knowledge of the type of system for which the antenna is to be designed, a ground wave radiating antenna is highly impractical, so using the GA as a tool to develop a space wave radiating wire geometry is a significant departure from any research ever conducted, to the author's knowledge.

III. Methodology

3.1 Overview

Now that the groundwork is in place for an understanding of the effect that the lossy earth has upon antennas and the promise of using genetic algorithms for electromagnetic design problems, the approach is presented. The approach is divided into three major divisions, or phases.

The first division entails the construction of two integrated GAs, algorithms which worked in concert with NEC4.1. The first of the integrated codes is titled the *simple genetic algorithm* (SGA) because it is based upon the fundamental principles behind the genetic methodology. The second of the two codes takes advantage of a GA software package developed by Zbigniew Michalewicz at the University of North Carolina called GENOCOP III, a highly sophisticated program developed over the course of seven years, and its associated integrated code will be known as the GENOCOP III-GA (GGA). Additionally, some issues in interfacing with the NEC4.1 code are investigated.

The second phase of this approach covers three different geometry definitions. The first is a relatively simple problem definition, that of a series-connected wire antenna, which is later used as a basis for comparision between the SGA and the GGA for the four-wire case. The second part of this divisions piggybacks on the first part but broadens the geometry definition for the wires, introducing the concept of the *wire-tree* antenna. For the GA runs in the wire-tree definition, a best configuration of the SGA is sought. Because of time constraints on the research, the GGA was not modified for a direct comparison to be made for this case. The final geometry definition is based on insight obtained from the results from the first two. In this phase, the wire geometry is constrained to that of a *vertical loaded monopole* (VLM) and then optimized using the SGA (also because of time constraints). It is this definition that leads to a final antenna design proposed for use in a RIMS.

The third and final division of the methodology is to detail the method for analyzing the genetically-derived designs. Important factors to consider are the polarization of the far-

field wave, the input impedance of the antenna, and the associated loss experienced by the antennas over the lossy ground. This phase shows how the *range improvement factor* metric is developed and how it indicates the quality of the genetic designs versus a typical RIMS antenna.

3.2 Integrated GAs

For *proof-of-concept* purposes, a basic GA was written in Fortran 77. The programming language was chosen in anticipation of interfacing the GA with the NEC4.1 code, which is also written in Fortran 77. Knowing in advance that the NEC4.1 code would have to be slightly modified, but not knowing to what extent, the fact that the two components of the integrated GA were written in the same language offered some hope for a quick and easy integration. As it turned out, the modifications made to NEC4.1 were minor. The starting point of the implementation is the creation of the integrated GAs. The sections that follow outline the setup.

3.2.1 Common Factors. Several setup characteristics are common to both the SGA and GGA. The wire geometry definitions were identical, as well as the type of ground used. From a GA perspective, other aspects of the integrated GAs had to be identical in order to make useful comparisions, particularly in the definition of features, constraint of feature values, string definition, and fitness calculation.

3.2.1.1 Domain Constraints. Based upon guidelines given by the sponsor, a constraint is imposed upon the wire geometry. The wires of the design are confined to a particular space defined in rectangular coordinates. The space is defined by

$$x_l \leq x \leq x_u \text{ (meters)} \quad , \tag{3.1}$$

$$y_l \leq y \leq y_u \text{ (meters)} \quad , \tag{3.2}$$

and

$$z_l < z \leq z_u \text{ (meters)} \quad, \tag{3.3}$$

where the coordinates have lower bounds defined by x_l, y_l, and z_l and upper bounds defined by x_u, y_u, and z_u.

3.2.1.2 Features. Many GAs discretize the problem domain in order to implement a binary encoding scheme for the feature values. Instead, this effort represents feature values with real numbers since the domain defined in Section 3.2.1.1 is by nature a continuous space. The benefit to this approach is that it avoids the possibility that an ideal location for a wire endpoint would be somewhere between two values represented with the binary code. Another advantage is that the actual implementation of the code is simpler and less execution time is required, as no requirement exists for encoding and decoding schemes. For this type of problem space, Linden showed that real-valued features can achieve better fitness scores than their binary counterparts with the least amount of computational expense (34:1706).

Each feature is simply the value for the endpoint of the associated wire in Cartesian coordinates. That is, the mth feature, g_m, is described by

$$g_m = \left(x_m, y_m, z_m \right) \quad, \tag{3.4}$$

the rectangular coordinates of the mth wire endpoints. For the first division of the approach, the wires are connected in series with the first wire beginning at the origin, $(0, 0, 0)$, and ending at (x_1, y_1, z_1). Continuing, the mth wire begins at $(x_{m-1}, y_{m-1}, z_{m-1})$ and ends at (x_m, y_m, z_m). For example, a four-wire antenna could be defined by the following coordinates:

Wire #1: $(0.000, 0.000, 0.000)$ to $(0.000, 0.140, 1.618)$,

Wire #2: $(0.000, 0.140, 1.618)$ to $(0.214, 0.484, 1.025)$,

Wire #3: $(0.214, 0.484, 1.025)$ to $(0.046, 0.327, 0.430)$,

and

Wire #4: $(0.046, 0.327, 0.430)$ to $(0.390, 0.171, 1.805)$.

3.2.1.3 Strings. The strings are defined by the number of wires in a particular design. Each string is represented by M features, where M is the number of wires in the design. For this choice, the nth string is then

$$c_n = (g_1, g_2, ..., g_M) \quad . \tag{3.5}$$

From the previous example the four-wire representation becomes

$$
\begin{aligned}
c_n \quad = \quad & (0.000, 0.140, 1.618, 0.214, 0.484, 1.025, \\
& 0.046, 0.327, 0.430, 0.390, 0.171, 1.805) \quad .
\end{aligned}
$$

3.2.1.4 Fitness Determination. Each antenna design string must be evaluated for its worth, designated the *fitness*. Computing the fitness for an antenna is not a trivial task since no one method is widely accepted in this area. Linden and Altshuler computed fitness according to Equations 2.9 and 2.10. The fitness of a design should define the desired properties of the solution antenna, as the GA approach is a method of synthesizing the desired traits of the antenna into an antenna design.

Those well-versed in antenna design understand that no single measure provides the worth of an antenna. Many figures-of-merit exist: power gain, directivity, impedance, efficiency, etc. The list is endless. In actuality, the worth of an antenna is critically dependent upon the type of application. For example, an antenna to be used for personal communications measures up to a far different standard than one which is to be used for radar. In a RIMS system, the key factors in designing the antenna, at least the ones that were chosen for optimization, are power gain, azimuthal symmetry of power gain and input impedance.

Unfortunately NEC4.1 is not designed to derive a single value that determines the worth of an antenna design. The code does, however, calculate the necessary building blocks for the fitness calculation. As mentioned previously, the goal is to combine the power gain, azimuthal

3-4

symmetry, and input impedance into a single, meaningful value. In optimization terms, this is a multi-objective approach. This is where the weighted sum approach enters into the picture.

Before the computation of a weighted sum, it is necessary for one to define the elements that will be weighted and summed, the individual objectives. The objectives of this research are power gain, a derived assessment of symmetry, and the two components of the antenna's input impedence, $Z_{in} = R + jX$, the resistance, R, and the reactance, X. The same impedance performance could have been achieved by optimizing VSWR, but by expanding the input impedance optimization into two objectives, the mechanism is in place to match to the specific characteristics of an operational matching network used at the feed point of a RIMS antenna.

Since the antennas of a RIMS system are located on the ground, and the RIMS user is particularly interested in improving the performance of the system's antennas in a direction along that ground, the first objective is the average gain as computed at 32 far-field locations in spherical coordinates. The 32 points were described by all combinations of four zenith angles and eight azimuth angles (θ and ϕ in the spherical coordinate system of Appendix A). The chosen zenith angles are $\theta = 89.80°$, $89.85°$, $89.90°$, and $89.95°$. The chosen azimuth angles are $\phi = 0°, 45°, 90°, 135°, 180°, 225°, 270°$, and $315°$. The NEC4.1 code calculates the average gain using

$$G_{ave} = \frac{4\pi}{\Omega P_{in}} \int_{\Omega} P_{\Omega}(\theta, \phi) \, d\Omega \quad , \tag{3.6}$$

where P_{Ω} is the radiated power density computed over the solid angle Ω, which is formulated by

$$P_{\Omega} = \frac{1}{2} R^2 \operatorname{Re}\{\mathbf{E} \times \mathbf{H}^*\} = \frac{R^2}{2\eta} |\mathbf{E}|^2 \quad . \tag{3.7}$$

To compute the electric field vector, $\mathbf{E}$, NEC4.1 numerical evaluates the Sommerfeld integral equations (35:32–69). The range is represented by the R term. Since this research is only concerned with the far field, the

$$\frac{e^{-jkR}}{R} \tag{3.8}$$

dependance is factored out of **E**, cancelling with the R^2 term in Equation 3.7. The term for the input power to the antenna, P_{in}, which is defined as the power *accepted* by the antenna is derived by

$$P_{in} = \frac{1}{2}\text{Re}\{VI^*\} \quad , \tag{3.9}$$

with V and I being the complex voltage and current at the feed.

To enforce azimuthal symmetry, an equation that looks vaguely familiar to a variance computation (without being weighted by the probability of each occurrence) and identical to Equation 2.9 is called the *deviation sum* and designated by

$$D = \sum_{\phi,\theta}(G(\theta,\phi) - G_{ave})^2 \quad . \tag{3.10}$$

In Equation 3.10, G_{ave} is the very same as that computed in Equation 3.6, and $G(\theta, \phi)$ is the value computed for the power gain at each θ and ϕ, using the equation

$$G(\theta,\phi) = 4\pi\frac{P_\Omega(\theta,\phi)}{P_{in}} \quad . \tag{3.11}$$

Because the average power gain calculation of Equation 3.6 by itself does not encapsulate the total value of the antenna, other objectives are necessary. The power gain is a ratio of radiated power to P_{in}. This figure of merit does not take into account the amount of power being drawn from the excitation source by the antenna. In reality, an antenna could have high power gain while reflecting much of the power from the source due to impedance mismatch. To counteract the GA's selection of antennas with high gain that reflect much of the power, the fitness function also incorporates optimization for the resistive and reactive components of the input impedence, Z_{in}, which is defined by

$$Z_{in} = \frac{V}{I} \quad . \tag{3.12}$$

Finally, the mathematical representation of the fitness is a weighted sum of the four objective functions,

$$fitness = \sum_{i=1}^{4} k_i f_i(t_i) \quad , \tag{3.13}$$

where k_i is a weight coefficient and $f_i(\cdot)$ is a function mapping the raw objective value, t_i, to the interval [0,1]. For the power gain objective, t_1, the mapping function is defined as

$$f_1(t_1) = 1 - \exp(-K_1 t_1) \quad . \tag{3.14}$$

For the objectives of symmetry (t_2), resistance (t_3), and reactance (t_4), the functional form of $f_i(\cdot)$ is

$$f_{i=2,3,4}(t_i) = \exp(-|t_i - S_i|/K_i) \quad . \tag{3.15}$$

Figure 3.1 shows each $f_i(t_i)$ and their associated values of S_i and K_i.

Each mapping function performs the necessary transformation from the raw value returned by NEC4.1 to a corresponding percentage which is multiplied by the associated weight coefficient. The choice of exponentials for the functions ensures that $0 \leq f_i(t_i) \leq 1$ for all possible raw values. The K_i terms are chosen *a priori* using knowledge of the raw values obtained during preliminary research phases. Conversely, each S_i represents a raw value that is a desirable characteristic of the antenna design. The raw azimuthal symmetry value is really a measure of asymmetry, so larger values correspond to designs that radiate less symmetrically. Therefore, $S_2 = 0.0$ enforces the azimuthal symmetry objective. Also, $S_3 = 50.0$ Ohms (Ω) to obtain higher fitness for designs with an input resistance of 50.0 Ω. Likewise, $S_4 = 0.0$ Ω because an input reactance of 0.0 Ω is desirable. It is common knowledge that many electromagnetic sources anticipate a load resistance equal to 50.0 Ω and a reactance of 0.0 Ω. The function shapes in Figure 3.1 show how this mapping scheme works. More desirable raw values return larger *mapped* values. Consequently, the larger *mapped* values translate into larger portions of the corresponding weights in the fitness sum of Equation 3.13.
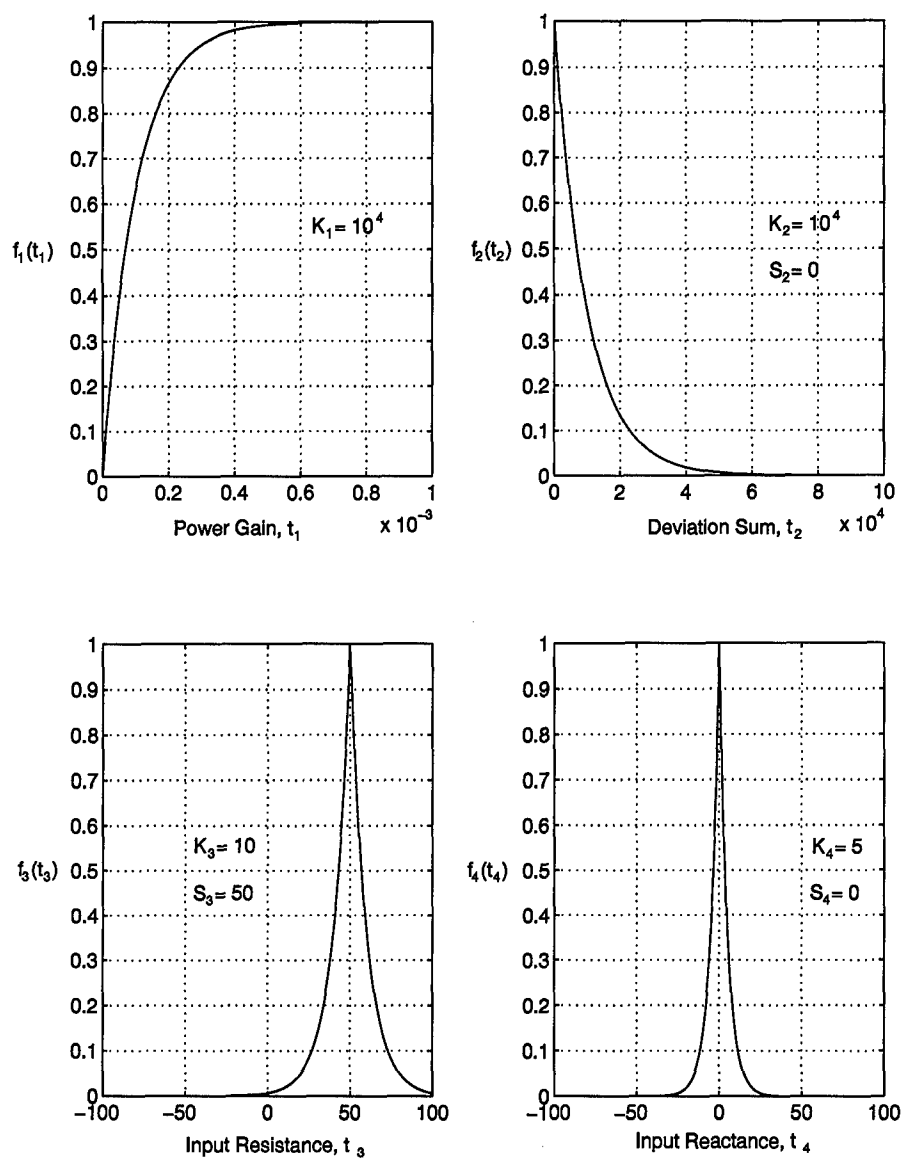
Figure 3.1   Objective Function Mappings

The weight coefficients were defined as $k_1 = 60$, $k_2 = 20$, $k_3 = 10$, and $k_4 = 10$. These values reflect that the power gain of the antenna is the most important objective of the design followed by the symmetry of radiated power. The choice of input impedance only comprising 20% of the fitness is not to say that input impedance is not important, just that for the purposes of this research, high gain is more desirable. The results presented in Chapter IV show this to be a wise decision. The choice of mapping functions and weights ensures all fitness values lie in the interval [0,100].

3.2.2 Simple GA (SGA).

3.2.2.1 Flow.
The SGA follows the basic flow of many of the basic GAs observed in the literature and is displayed in Figure 3.2. The feature values are generated with a uniform random number generator inside the domain constraints of Equations 3.1, 3.2, and 3.3. Fitness determination is discussed in Section 3.2.1.4. Instead of applying convergence criteria, a generational limit dictates the number of fitness evaluations performed in each run of the SGA. The remaining blocks from Figure 3.2 are discussed in the sections that follow.

3.2.2.2 Selection.
After the cost of each chromosome is evaluated, the SGA sorts the population so the greatest fitness is at the top. One method of selection coded into the SGA was elitist, where the top two strings are chosen to be the first crossover pair, the third and fourth ranking strings become the next, and so on until the top 40% of the population has been selected to repopulate the bottom 60%. The second method of selection was a four-member tournament, where four members of the top 20% of the pool were randomly chosen, and the two with the highest fitness become the crossover pair. This process is repeated until enough pairs are selected to repopulate the bottom 60% of the population.

One problem with non-random selection methods such as elitist is that a great deal of *selection pressure* occurs since crossover occurs only among the fittest strings (36:1699). Because of similarities between the fittest strings, the GA may converge to a sub-optimal solution, so Mohammed proposes using schemes incorporating random selection and/or fitness
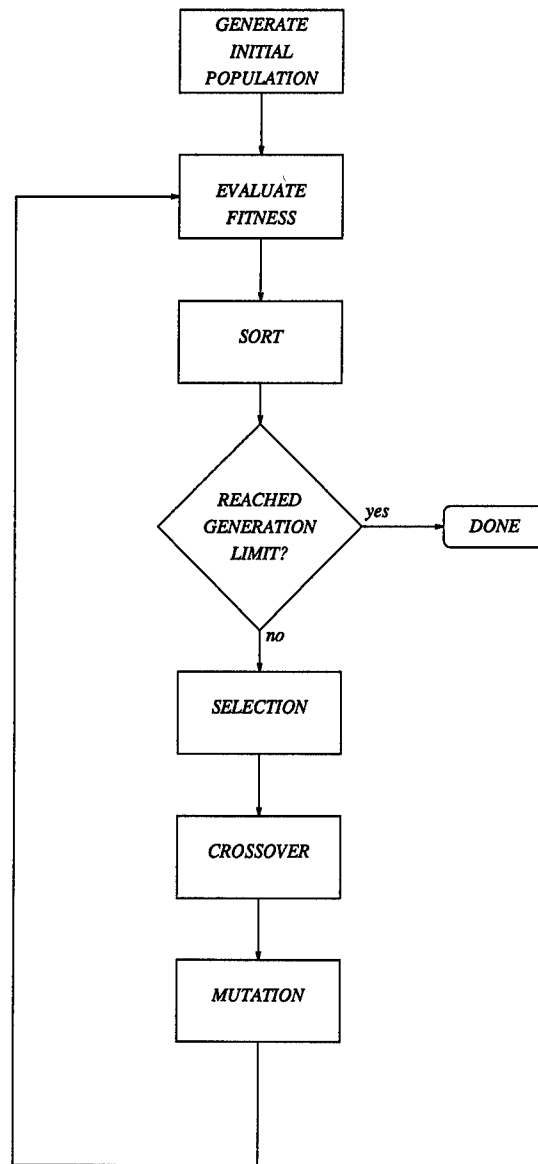
Figure 3.2   Flow Chart of the SGA

scaling to reduce this possibility (36:1699). Mohammed wavers on this matter, though, by stating that the random schemes may also be the cause of sub-optimal performance (36:1699). By directly comparing the results of elitist and tournament selection schemes in the SGA, this research will indicate a preferable method for this problem space.

3.2.2.3 Crossover. Crossover is a simple linear averaging scheme producing three individuals, where if C_p and C_q represent the two non-identical chromosomes selected for crossover, the resulting chromosomes, C_a, C_b, and C_c are found by

$$C_a = \frac{C_p + C_q}{2} \quad , \tag{3.16}$$

$$C_b = \frac{3C_p + C_q}{4} \quad , \tag{3.17}$$

and

$$C_c = \frac{C_p + 3C_q}{4} \quad . \tag{3.18}$$

The crossover scheme has a physical representation. It is designed to search the space between wire endpoints, and was inspired by the crossover scheme used by Yan and Lu for sidelobe reduction of array patterns (37:1119).

3.2.2.4 Mutation. Mutation allows the opportunity for the GA to more thoroughly search the landscape, possibly allowing it to find a global optima. The SGA implements mutation only for the strings produced by crossover, thus preserving the better performing members of the population. Two schemes were implemented, one in which one coordinate in each design was regenerated, called low (L). The second scheme was called high (H), where all three points in a wire endpoint were regenerated. The corresponding mutation rates are dependent upon the number of wires in the geometry.

3.2.3 GENOCOP III-GA (GGA). One of the advantages of GENOCOP III over the SGA is that it makes available a number of different operators for crossover and mutation.

The bottom line is that the larger variety of operators promotes a more thorough search of the landscape.

The number of times each operator is used by GENOCOP III is a random selection, but the code allows the user to define the distribution. For integration into the GGA, each of the three crossover and five mutation operators were assigned equal weights, forcing a uniform distribution. For this research, the crossover operators used were whole arithmetical, simple arithmetical, and Heuristic. The mutation operators were whole uniform, boundary, non-uniform, whole non-uniform, and Gaussian. The exact function of each of these operators is explained by Kaiser (38:91–94).

An exhaustive explanation of the GENOCOP III algorithm is beyond the scope of this research effort. However, more information can be learned about GENOCOP III in the work of Michalewicz and Nazhiyath (39:647-651).

3.2.4 Interfacing With NEC4.1.   Being a MoM code, NEC4.1 checks input wire geometries to ensure the accuracy of the MoM solution. Appendix C documents the MoM approach. In the context of using NEC4.1 to determine fitness of a wire design, geometries that produce inaccurate MoM solutions cannot be used by the GA. In the event that NEC4.1 identifies a problem geometry, the fitness routine identifies the occurence and labels the geometry erroneous. In this way, the problem geometry is *infeasable*. By marking infeasable designs with zero fitness, the GA will converge to feasable designs.

An important consideration in using NEC4.1 with a lossy earth condition is with regard to how large the segments must be. The wires must be divided into segments proportional to their λ in the earth medium, not the λ in free space (40:12). Segment lengths were chosen to be no greater that 5% of the wavelength in the lossy medium.

3.3 Geometry Definitions

3.3.1 Series Geometry.

For a first-look at how the SGA and GGA perform in this area, the space is chosen to be a rectangular box above the x-y plane, with

$$x_l = y_l = -0.5 \,(\text{meters}) \quad , \tag{3.19}$$

$$x_u = y_u = 0.5 \,(\text{meters}) \quad , \tag{3.20}$$

$$z_l = 0.001 \,(\text{meters}) \quad , \tag{3.21}$$

and

$$z_u = 2.0 \,(\text{meters}) \quad . \tag{3.22}$$

Note that the lower bound of z is set to 1 mm. The reason for this lower bound on z is two-fold. First, this constraint keeps the wires above the ground, which is desirable since the lossy earth absorbs much of the power for a buried wire. Second, the tolerance is established on the order of millimeters in consideration of manufacturing tolerances for a wire antenna of this type. A smaller tolerance would be difficult to manufacture and impossible to maintain. It is desirable for the lower bound to be as close to the ground plane as possible, so 1 mm is the logical choice.

3.3.2 Extended Geometry: The Wire-Tree.

Forcing the wires to be series connected leads to a very limited solution space. To enlarge the space of wire geometries, the concept of a wire-tree is introduced. For a more complete visualization of the constraints imposed on the GA, an analogy is made between the wire geometry and a biological tree. As in Section 3.2.1.3, a number, M, of series-connected wires are generated to form the *trunk* of the antenna. At each of the $M - 1$ points on the antenna where two trunk wires meet, a *branch* consisting of B wires is connected. The purpose for incorporating branches into the design is to promote more coupling between the wires, making impedence matching more likely.

By redefining the geometry, the string that represents each geometry is redefined and becomes a matrix instead of a vector. The new string matrix is represented by

$$c_n = \begin{bmatrix} g_1 & g_2 & \cdots & g_{M-1} & g_M \\ g_{1,1} & g_{2,1} & \cdots & g_{M-1,1} & \emptyset \\ g_{1,2} & g_{2,2} & \cdots & g_{M-1,2} & \emptyset \\ \vdots & \vdots & \ddots & \vdots & \vdots \\ g_{1,B} & g_{2,B} & \cdots & g_{M-1,B} & \emptyset \end{bmatrix} \tag{3.23}$$

where B indicates the number of wires in each branch. In the last column of c_n, all elements but the first are ignored with the existing constraint that branches only connect to the interior nodes of the trunk. Using this new string definition, the wires are connected according to Figure 3.3.
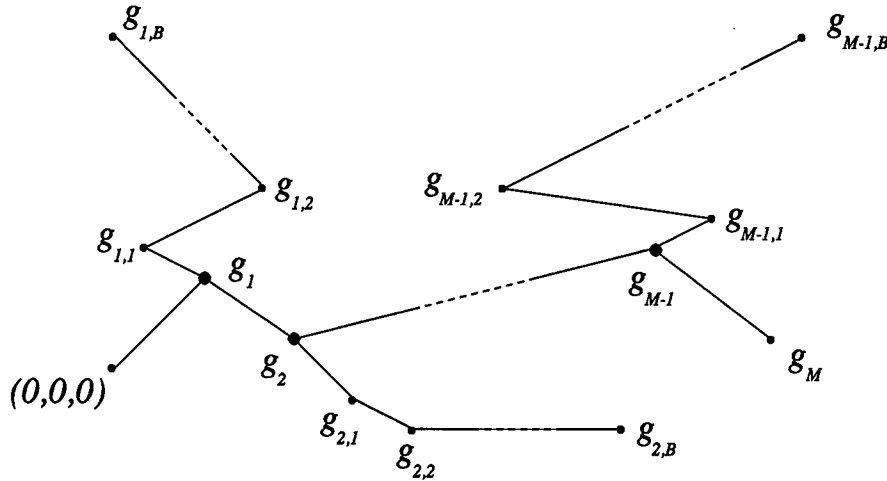
Figure 3.3　Definition of Wire-Tree Antenna String

Preliminary research indicated that the GGA was superior to a version of the SGA (41:6). The configuration scheme of the SGA that was chosen to compete directly with the GGA was chosen after a cursory investigation of its performance versus the other configurations. This investigation was not thorough enough to determine that the configuration was well-suited to the problem space. Therefore, a further investigation is necessary.

For the sake of computational expense, the problem was scaled to smaller dimensions. The space chosen was define by the bounds

$$x_l = y_l = -0.25 \text{ (meters)} \quad , \tag{3.24}$$

$$x_u = y_u = 0.25 \text{ (meters)} \quad , \tag{3.25}$$

$$z_l = 0.001 \text{ (meters)} \quad , \tag{3.26}$$

and

$$z_u = 0.75 \text{ (meters)} \quad . \tag{3.27}$$

In terms of wavelength at the center frequency of the band of interest, 145.5 MHz, these distances correspond to

$$-0.12\lambda \le x, y \le 0.12\lambda \tag{3.28}$$

and

$$0.00\lambda \le z \le 0.36\lambda \tag{3.29}$$

The limiting of these to the electrically small region significantly reduces computation time but poses no problem with the accuracy of the NEC4.1 solution (40:5). To further reduce the computation time for the iterations, the only geometry considered was two wires connected in series ($M=2$, $B=0$).

All ten trials of SGA that is compared to the GGA in Section 4.2 converged before the twentieth generation, that is to say that any fitness gains occurring after the twentieth generation were relatively small. This result became a good starting place to restrict this investigation so that it could be carried out in an reasonable amount of time. Beginning with an initial population of 50 strings and allowing iteration for 20 generations equates to 620 fitness calculations. With a similar restriction on the total number of fitness evaluations, populations of 155 and 20 strings were allowed to iterate for 6 and 51 generations, respectively.

Mutation	Fitness											
Population Size	20				50				155			
Selection Type	Elitist		Tournament		Elitist		Tournament		Elitist		Tournament	
Mutation	Low	High	Low	High	Low	High	Low	High	Low	High	Low	High
Run #1	65.0	62.4	63.7	61.7	65.9	62.1	57.1	60.1	67.0	60.1	62.0	59.6
Run #2	62.7	62.4	63.9	61.1	64.6	60.8	58.2	57.2	63.4	58.2	58.1	61.8
Run #3	57.8	61.8	64.1	61.4	65.4	62.0	57.0	57.6	64.7	58.0	65.6	61.8
Run #4	67.0	65.3	66.4	61.8	66.8	61.1	57.8	59.3	66.4	60.2	66.0	61.2
Run #5	58.6	62.1	64.7	60.0	65.4	62.4	56.3	60.5	65.5	58.4	63.3	61.8
Run #6	65.0	62.2	63.4	61.2	60.1	61.1	57.2	60.6	66.1	61.4	57.3	58.2
Run #7	64.3	62.4	64.3	65.7	67.0	62.0	57.1	59.5	57.4	62.4	66.1	60.5
Run #8	63.9	61.8	61.3	61.2	66.1	62.3	57.7	62.2	64.9	60.7	57.1	61.7
Run #9	65.1	61.0	64.8	61.8	58.4	61.1	60.2	61.4	66.7	61.1	65.8	58.6
Run #10	62.7	62.3	65.1	61.4	61.5	61.6	56.1	58.7	66.7	60.4	57.3	60.4

Table 3.1 **Experiment Matrix for Determining the Best Configuration of the Simple Genetic Algorithm (SGA)**

The investigation sought to find the best way to use the SGA. All combinations of the SGA settings for selection and mutation are shown in Table 3.1 for the trials which were performed for the three separate population sizes mentioned previously.

For population sizes that are relatively large with a fixed number of fitness evaluations, the mean value of the elite-selection, low-mutation (E-L) SGA is much higher than that of any other configuration as shown in Figure 3.4. Note that the mean value of the E-L configuration has an upward trend with increasing population size. The tournament-selection, low-mutation (T-L) scheme also has an upward trend but produces lower mean values. Another promising aspect of the E-L method is the relative independence of its mean with population size.

The E-L configuration also shows promise when the variance of fitness values is investigated and is consistent regardless of population size. The T-L scheme shows a high degree of variance for a population size of 155, which leads one to believe that its mean value in Figure 3.4 was somewhat anomalous, and the upward trend witness is suspect.

Based on the evidence in Figures 3.4 and 3.5, the best configuration for this problem's space was the combination of elitist selection and low mutation. This configuration of the SGA was used for genetically optimizing the remaining two geometry definitions.
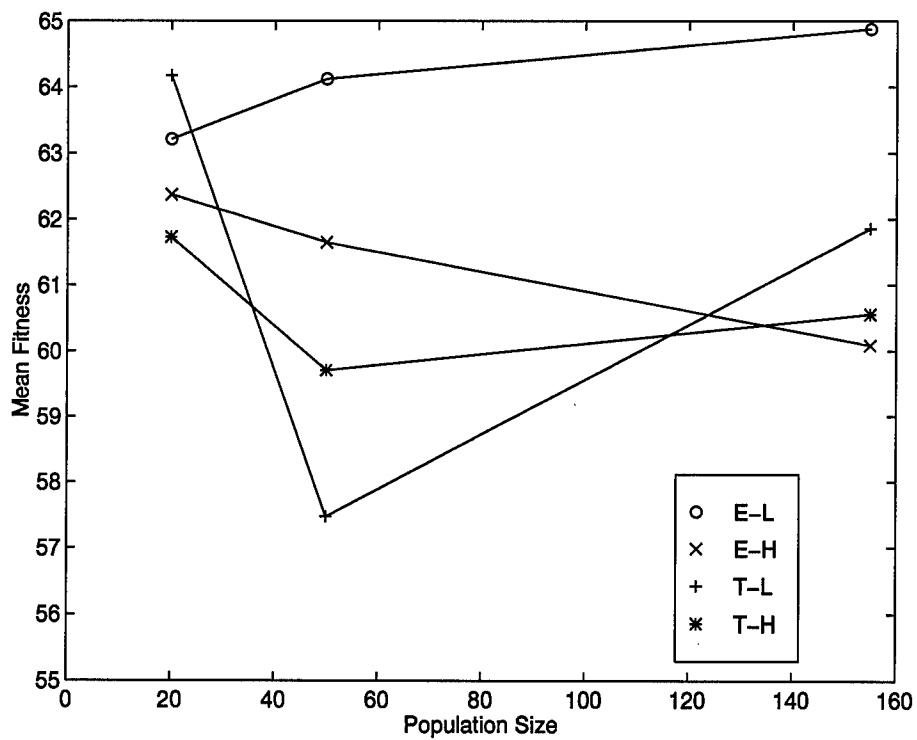
Figure 3.4   Average Fitness Value for the Four Different SGA Configurations of Selection (E: Elitist, T: Tournament) and Mutation (L: Low, H: High)
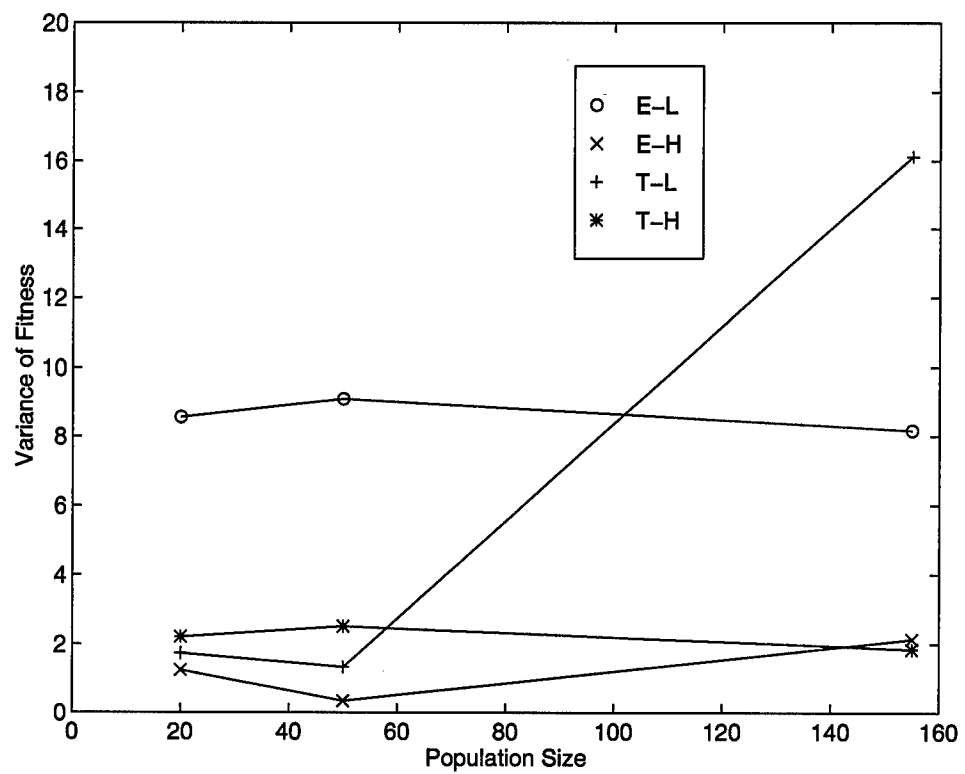
Figure 3.5   Variance of the Fitness Values for the Four Different SGA Configurations of Selection (E: Elitist, T: Tournament) and Mutation (L: Low, H: High)

3.3.3 Symmetrical Geometry: The Vertical Loaded Monopole (VLM). Based on the types of results that were obtained by both the SGA and the GGA in the early stages of research, a third type of geometry was investigated, that of a *vertical loaded monopole* (VLM). In this geometry definition, the first wire, that connected to the source, was restricted to be completely vertical. Then, four equal-length wires were symmetrically attached to the vertical wire for the purpose of loading.

This definition led to re-defined string, that of only four features, defined by

$$c_n = (z_1, z_2, w, z_3) \quad , \tag{3.30}$$

where the geometry is defined in Figure 3.6.

3.4 Analysis

The analysis of the proposed antennas is relatively simple, since most of the calculations are performed by NEC4.1. A short overview of the computational methods employed by NEC4.1 is available in Appendix C. An exhaustive description of the methods employed by NEC4.1 is available from Burke (35:1–142).

3.4.1 Link Budget. The NEC4.1 code is not designed to perform all of the necessary analysis that antenna design requires. The *big picture* is not obtained by simply plotting the values of impedance and the radiation pattern as computed by the code. True benefit is obtained by performing a power budget analysis of the antenna, which takes into account a particular receive antenna—this research is focused on designing a transmit antenna—and the factors of radiated power, polarization mismatch, and impedance mismatch. This type of analysis is imperitive to the assessment of the proposed antenna. Slightly modified from Stutzman and Thiele (42:69), the power delivered to the load is

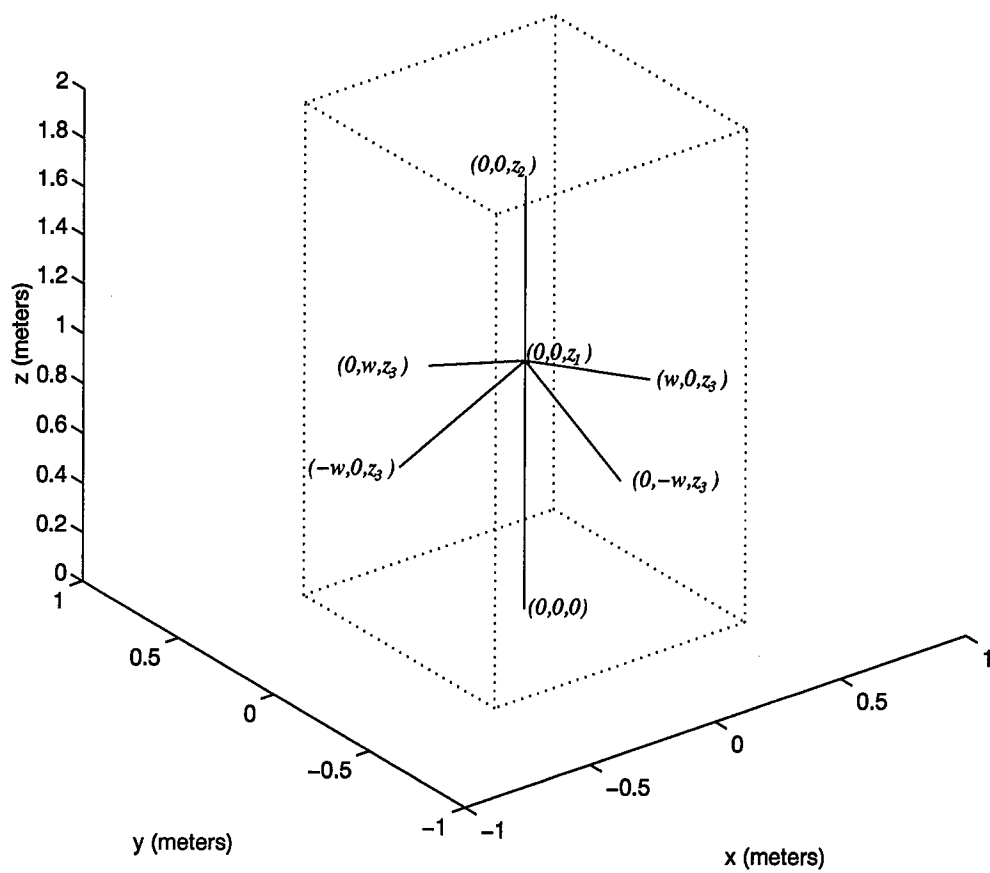$$P_D(\text{dBm}) = P_R(\text{dBm}) + p(\text{dB}) + q(\text{dB}) \tag{3.31}$$

Figure 3.6   **Symmetrical Geometry Definition**

where P_D is the power (in decibels above a milliwatt) delivered to the load, P_R is the total radiated power (in decibels above a milliwatt), p is the *polarization mismatch loss* (in decibels), and q is the *impedance mismatch loss*(in decibels). The following sections cover the loss terms in detail.

3.4.1.1 *Polarization Mismatch Loss.*   Polarization mismatch loss, p, is defined mathmatically as

$$p = |\hat{\mathbf{h}}_R^* \cdot \hat{\mathbf{e}}|^2 \quad ,$$

(3.32)

where $\hat{\mathbf{h}}_R$ and $\hat{\mathbf{e}}$ are complex unit vectors for the receiving antenna's effective length and for the impinging wave, and $*$ is the complex conjugate operator. These vectors are written as

$$\hat{\mathbf{h}}_R = \hat{\phi} \, \cos \gamma_R + \hat{\theta} \, \sin \gamma_R \, e^{j\delta_R} \quad ,$$

(3.33)

and

$$\hat{\mathbf{e}} = \hat{\phi} \, \cos \gamma_I + \hat{\theta} \, \sin \gamma_I \, e^{j\delta_I} \quad ,$$

(3.34)

where the parameters that characterize the elliptical polarization for the incident wave and the receiving antenna, γ and δ, are discussed in Stutzman and Thiele's text (42:55–56) and given by

$$\gamma = \arctan \left(\frac{E_\theta}{E_\phi} \right)$$

(3.35)

and

$$\delta = \arccos \left(\frac{E_\theta^2 - E_\phi^2}{2 E_\theta E_\phi} \tan 2\tau \right) \quad ,$$

(3.36)

and E_θ and E_ϕ are computed by NEC4.1 and appropriately chosen for the incident wave (noted by the I subscripts on γ and δ) and the receiving antenna (noted by the R subscripts on γ and δ). The NEC4.1 code also computes the tilt angle, τ.

3.4.1.2 Impedance Mismatch.   The amount of loss due to impedance mis-match is given as

$$q = 1 - \frac{|Z_o - Z_{in}|^2}{|Z_o + Z_{in}|^2} \quad , \tag{3.37}$$

where Z_o is the characteristic impedance of the transmission line feeding the antenna (assumed to be 50 Ω in this research).

3.4.2 Range Improvement Factor.   Even with the link budget, it is not clear how a particular antenna will improve the performance of a RIMS. The analysis should boil down to the single metric of interest—range. For propagation at low elevation angles, how much improvement in range over the current system does an antenna provide? The metric that provides this information is the *range improvement factor*, κ, such that the range of the antenna designed using a GA, R_{GA} is simply the range of the monopole, R_M multiplied by a factor κ, which is represented mathmatically as

$$R_{GA} = \kappa R_M \quad . \tag{3.38}$$

The formulation of κ begins with the simple form of the one-way radar range equation,

$$R^2 = \frac{P_t G_t G_r q^2 p}{4\pi P_r} \quad , \tag{3.39}$$

where the terms for power (P) and gain (G) are appropriately modified by the subscripts r and t for the receiving antenna and the transmitting antenna. Due to the reciprocity theorem, the q term is raised to the second power in Equation 3.39 because the same loss is experienced a both transmit and recieve ends when the same antenna is used (42:44). The p term is only experienced at the recieve end and thus is only raised to the first power. The power terms represent the power available at the input (in the case of the transmitting antenna) and output (receiving antenna) terminals.

A RIMS uses the $\lambda/4$ vertical monopole for both the transmit and receive ends of the system. An assumption in this derivation is that this monopole is perfectly matched, so $q = 1$.

3-22

In addition, the vertical monopole system, which radiates only a θ-directed electric field, suffers no polarization loss, making $p = 1$ also. From this, the range of the monopole is described as

$$R_M^2 = \frac{P_t G_M G_M}{4\pi P_r} \quad .$$

(3.40)

For the genetic antenna, no assumptions are made about losses, leading to

$$R_{GA}^2 = \frac{P_t G_{GA}^2 q_{GA}^2 p_{GA}}{4\pi P_r} \quad .$$

(3.41)

Using Equation 3.38 to combine Equations 3.40 and 3.41, κ is then formulated to be

$$\kappa = \frac{G_{GA} q_{GA}}{G_M} \sqrt{p_{GA}} \quad .$$

(3.42)

3.5   Onward

With the establishment of two integrated GAs, the SGA and the GGA, it is time to move forward to the Chapter III to see the results of the optimization procedure for the three different geometry definitions and see how the genetic designs perform as antennas, particularly when compared to a typical RIMS antenna.

IV. Analysis

4.1 Analysis of λ/4 Monopole

Before moving forward to the analysis of any of the GA-designed wire antennas, the performance of the type of antenna often used in a RIMS must be modeled. Such analysis establishes a baseline for comparison and allows an intelligent assessment of the performance capabilities of the proposed design. In order to perform such comparisons, a level playing field must be established. Factors like frequency, excitation source, ground plane, wire radius must be the same for all designs.

4.1.1 Developing the Model.

4.1.1.1 Frequency.
The frequency band designated by the Federal Communications Commission (FCC) for unattended sensors is 138–145 MHz. It is quite possible that the location of an operational RIMS system would not be under the auspices of the FCC, but some locales may reside within FCC juristiction. For example, test requirements may force a RIMS's performance to be evaluated in the United States. Therefore, compliance is absolutely necessary.

A typical RIMS antenna is a λ/4 length monopole. The physical length is specified by the center frequency of the band, 145.5 MHz, making it 0.515 meters long. In a like manner, the GA designed antennas were designed for the center frequency of the band and analyzed over the entire band.

4.1.1.2 Excitation Source.
Modeling the excitation source of the antenna is a critical equalizing factor. NEC4.1 offers two models for sources. As with any moment method code, the accuracy of source modeling dictates the accuracy of the computed impedance and gain for the antenna (35:6). The simplicity and reliability of the applied-field source model makes it an easy choice for selection as the modeling mechanism in this application, particularly

because the wire radii are electrically small (approximately $\lambda/5000$), and the effect of the actual feed structure on the input impedance will be negligible (35:76).

Since the assumption was made in Section 1.6.5, it is important to note the effect of a source located on the ground. For all antennas modeled in this research, the earth, with its specified electrical characteristics, ϵ_r and σ, is one end of the gap to which the voltage is applied. This, in effect, connects the signal generation circuitry ground to that of the real earth and is important for realistic impedance calculations.

4.1.1.3 Wire Modeling. The wire radius was kept constant throughout the research. Although NEC 4.1 is capable of treating stepped radius wires, adding variability to the wire radius was not a consideration. With typical wire radii in RIMS applications being excruciatingly small fractions of a wavelength, to allow wire radius fluctuation enough to impact the design would cause the design context to be violated. The bottom line is that thin wires must be used to avoid visual detectability.

The wire radius for all wires in the design is a fixed value of 0.4 mm. The purpose of this choice is two-fold. One, this is close to the radius of wires typically used in modern systems. Two, the radius is thick enough that wires should be able to maintain the structure geometry without jeopardizing the intended function of the antenna. Realistically, since the wire radius is such a small fraction of the wavelength, the wire radius is not a major factor.

4.1.2 Input Impedance. Figure 4.1 shows the resistive and reactive componenents of the input impedance for the $\lambda/4$ monopole over two types of earth surface. Two types of ground were chosen for comparison. From Appendix B, a key term in the complex reflection coefficient is $\sigma/\omega\epsilon$. Therefore, the values for the ground parameters in Figure 4.1 were chosen to have large and small values for $\sigma/\omega\epsilon$. The first type of ground falls within Kraus's quasi-conducting region with values of $\epsilon_r = 30$ and $\sigma = 111$ $m\mho/m$ (43:548–549). The second type of ground falls within the dielectric ground region with values of $\epsilon_r = 15$ and $\sigma = 0.04$ $m\mho/m$ (43:548–549). Note that at 145.5 MHz, all types of solid earth fall into the dielectric or quasi-conducting regions—none act like a conductor (43:549). The

large change in the ground type has a only a minor impact on the input impedance shown in Figure 4.1 due to the fact that the voltage is connected to the ground and NEC4.1 interpolates the currents to the image in the ground plane.
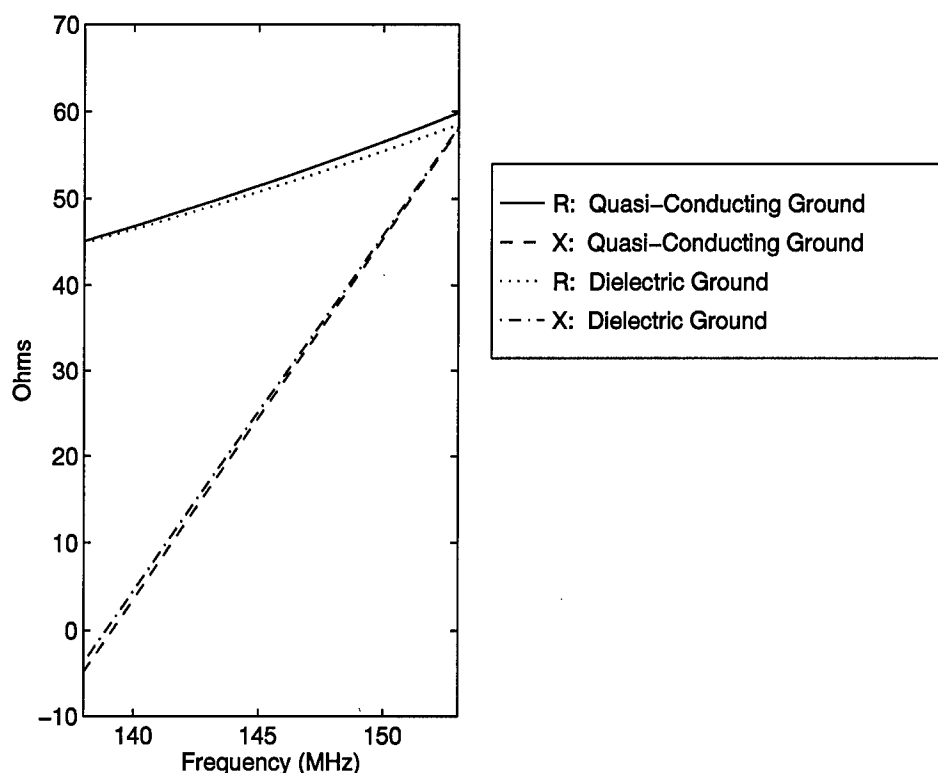

Figure 4.1   Components of the Input Impedence for the λ/4 Monopole in the Presence of Two Types of Ground: Quasi-Conducting ($\epsilon_r = 30, \sigma = 111$ m℧/m) and Dielectric ($\epsilon_r = 15, \sigma = 0.04$ m℧/m)

4.2   Series Geometry Results

For the runs incorporating the basic geometry defined in Section 3.3.1, the choice of $M = 4$ allowed some complexity to enter the design while keeping the number of wires to a reasonable level to avoid a messy conglomeration of wires. For this simple geometry, the antennas obtained by both the SGA and GGA are directly compared. In order to make a comparison, the number of fitness evaluations was limited for each algorithm. For the SGA, a population of 50 strings was used and it was allowed to iterate for 100 generations, resulting

	Best Fitness	
Run #	SGA	GGA
1	70.1	75.5
2	72.4	73.0
3	69.8	69.8
4	70.1	78.8
5	70.0	70.2
6	70.1	73.2
7	60.1	75.5
8	70.0	74.2
9	70.1	78.7
10	70.0	70.4
Mean (μ)	69.3	73.9
Variance (σ^2)	9.9	9.6

Table 4.1   **Comparison of SGA and GGA Results for the Four-Wire Series-Connected Geometry**

in a total of 3020 fitness evaluations. Similarly, the GGA was limited to a maximum of 3020 fitness evaluations. The results of this experiment involved 10 unique runs for both GAs. The best fitness obtained by each of the GAs for each run is shown in Table 4.1. The superiority of the GGA is evident by a significantly higher mean and a lower variance in the trials. This result proves that the variety of crossover and mutation operators used by GENOCOP III performs a more adequate search of the landscape.

4.2.1 Optimized Geometries.   From the second run of the SGA, the antenna with the highest fitness is displayed in Figure 4.2. The antenna with the highest fitness found by the GGA came from the fourth run and has a geometry shown in Figure 4.3. By simply looking at the geometry, it is not perfectly clear why this antenna performs better than any other arbitrary conglomeration of wires. However, the GGA design exhibits some definite characteristics that would be expected for this application. A mostly vertical element rises from the source and is augmented by some sort of top-loading structure. The SGA design is a little more peculiar but still exhibits the height characteristic.
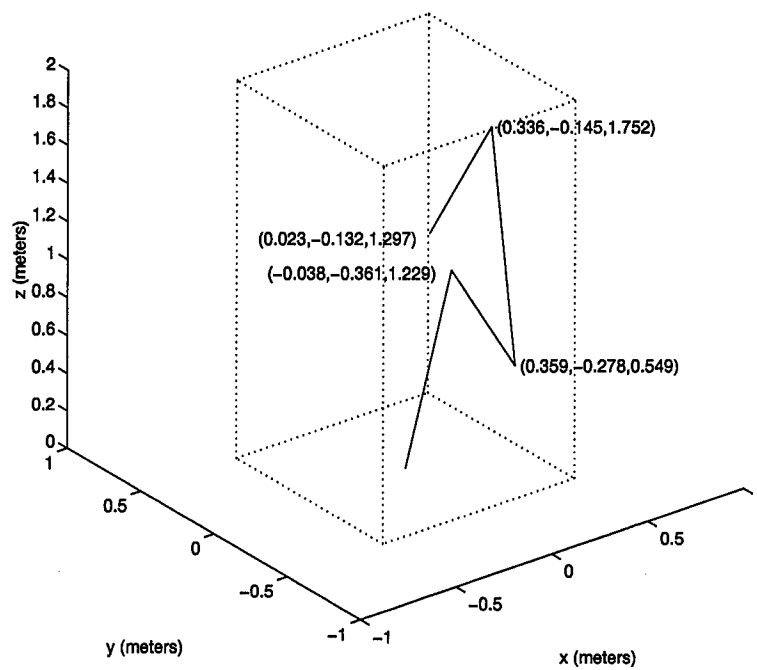
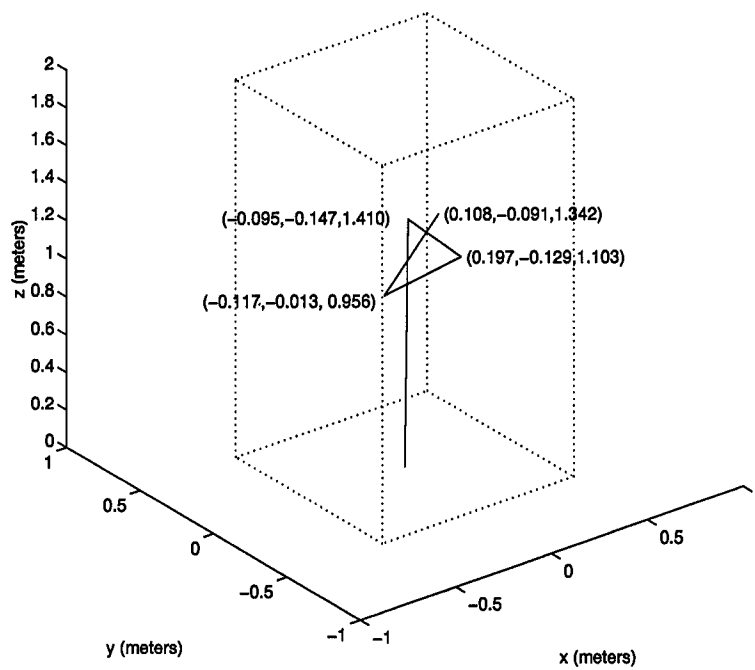Figure 4.2   Four-Wire Geometry Found by SGA

Figure 4.3   Four-Wire Geometry Found by GGA

4.2.2 Power Gain. Elevation cuts of the power gain as computed by Equation 3.11 are shown in Figures 4.4 through 4.11. On each plot, the gain of the $\lambda/4$ monopole is also given to provide the opportunity for a direct visual comparison with the GA designs.
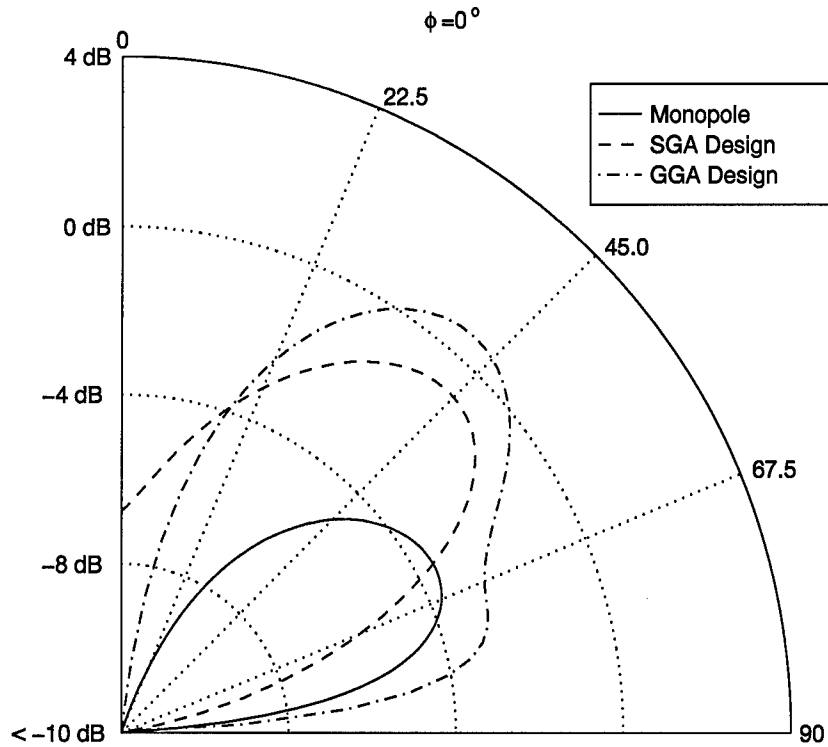

Figure 4.4 **Four-Wire Geometry: Elevation Cut of Power Gain at an Azimuth of $\phi = 0°$**

The power gain plots in Figures 4.4 and 4.5 are particularly disturbing from a user point-of-view because they show a major deficiency in the SGA design. For angles of $\theta > 67.5$, the monopole gain is at least 4 dB greater than the SGA design. For the other azimuth cuts given, this deficiency is not present, but it is this lack of symmetry in the SGA design that differentiates it from the GGA design by a lower fitness score.

The symmetry of the gain for the GGA design is very good considering its asymmetrical geometry. This result is attributable to its long, mostly-vertical wire which serves a monopole function. The height of the vertical wire in the GGA design is greater than that of the RIMS monopole by nearly a meter, which explains its superiority in gain at the lower elevations.
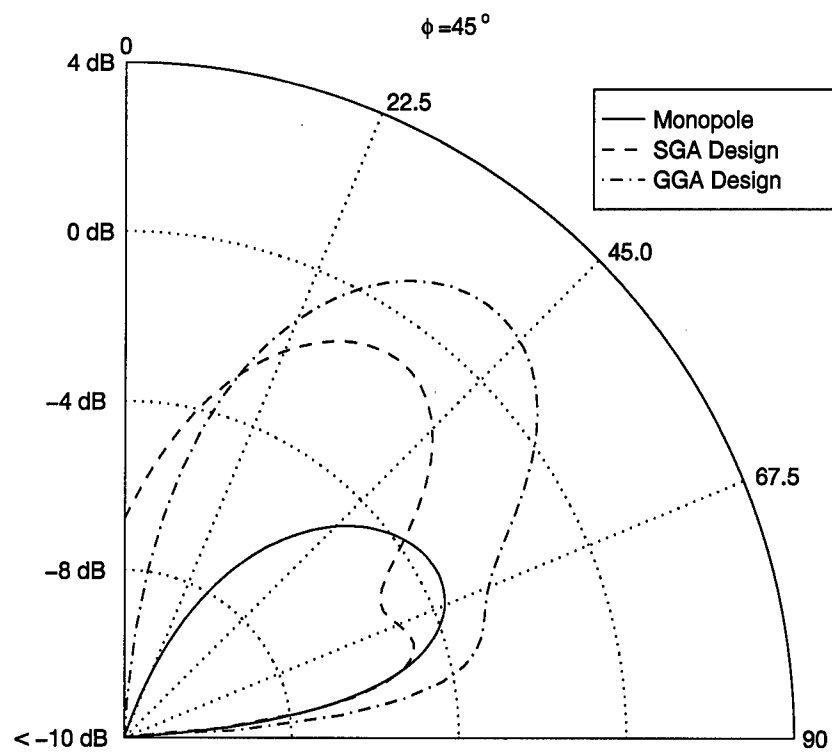
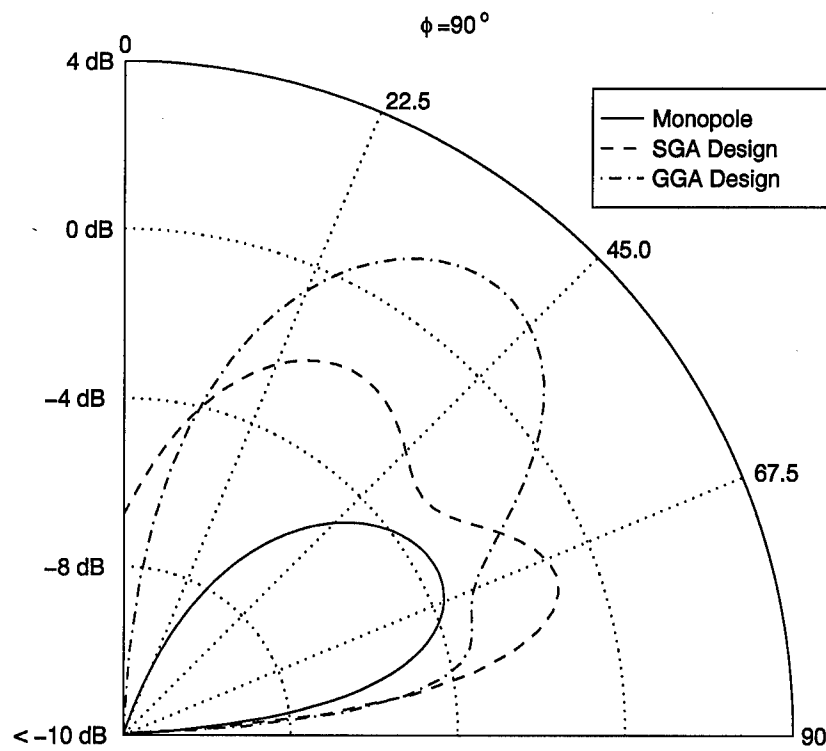Figure 4.5 **Four-Wire Geometry: Elevation Cut of Power Gain at an Azimuth of** $\phi = 45°$

Figure 4.6   Four-Wire Geometry: Elevation Cut of Power Gain at an Azimuth of $\phi = 90°$

For the GGA design at most all of the azimuth positions, the GGA design offers a 1 dB improvement in power gain over the monopole at $\theta = 67.5°$. This improvement increases to approximately 4 dB at $\theta = 82°$.
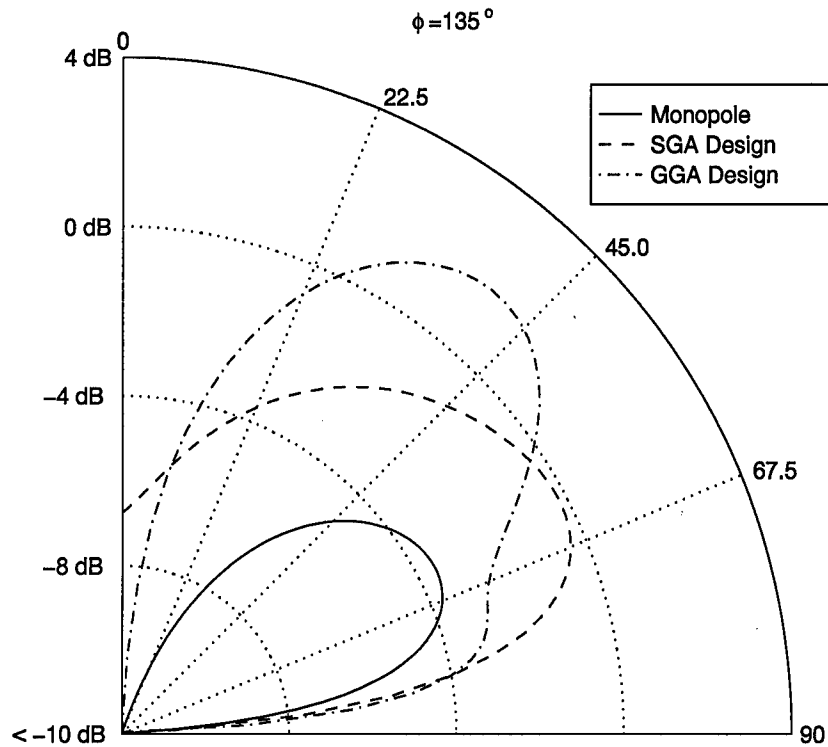

Figure 4.7   Four-Wire Geometry: Elevation Cut of Power Gain at an Azimuth of $\phi = 135°$

At several azimuth positions, the SGA design exhibits better gain (up to 3 dB for $\theta > 67.5$), particularly at $\phi = 90°$, $135°$, $270°$, and $315°$. However, this does not make the SGA design a better antenna for the RIMS application because of the previously discussed lack of symmetry in its gain patterns.

An interesting observation about the SGA pattern at an azimuth of $\phi = 180°$ is that the null around $\theta = 0$ is filled. This filling occurs because of the more horizontally-oriented wires in the geometry, which have strong radiation characteristics reminiscent of horizontal dipoles near a ground plane.

Figure 4.8 Four-Wire Geometry: Elevation Cut of Power Gain at an Azimuth of $\phi = 180°$

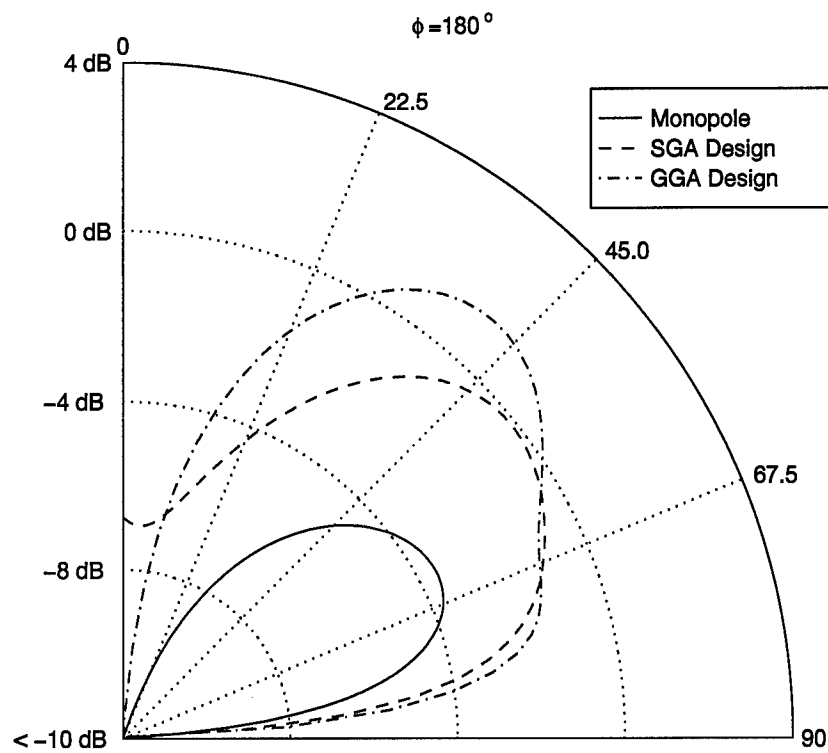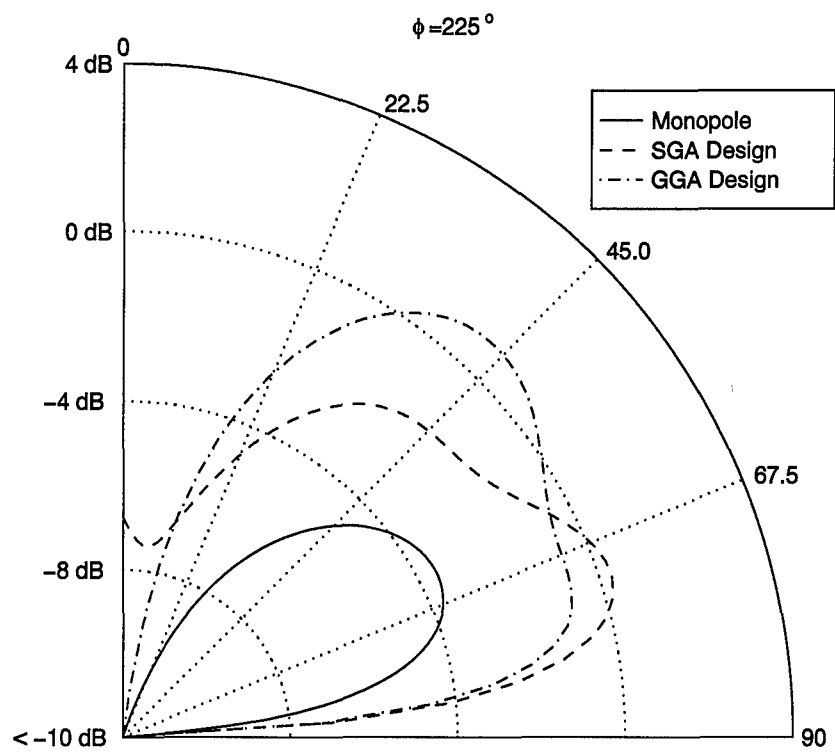Figure 4.9   Four-Wire Geometry: Elevation Cut of Power Gain at an Azimuth of $\phi = 225°$

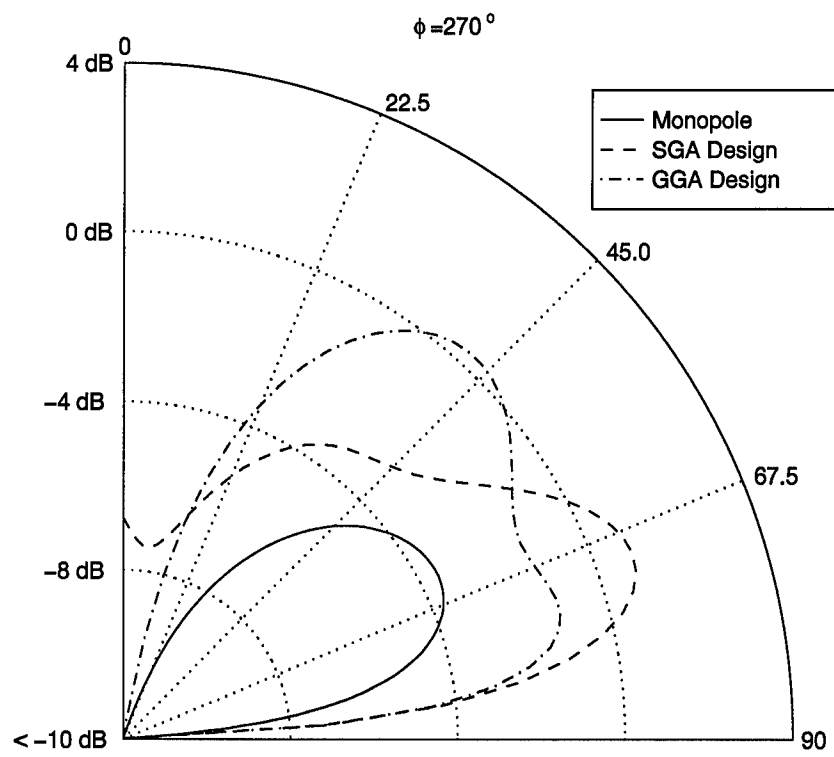**Figure 4.10   Four-Wire Geometry: Elevation Cut of Power Gain at an Azimuth of $\phi = 270°$**
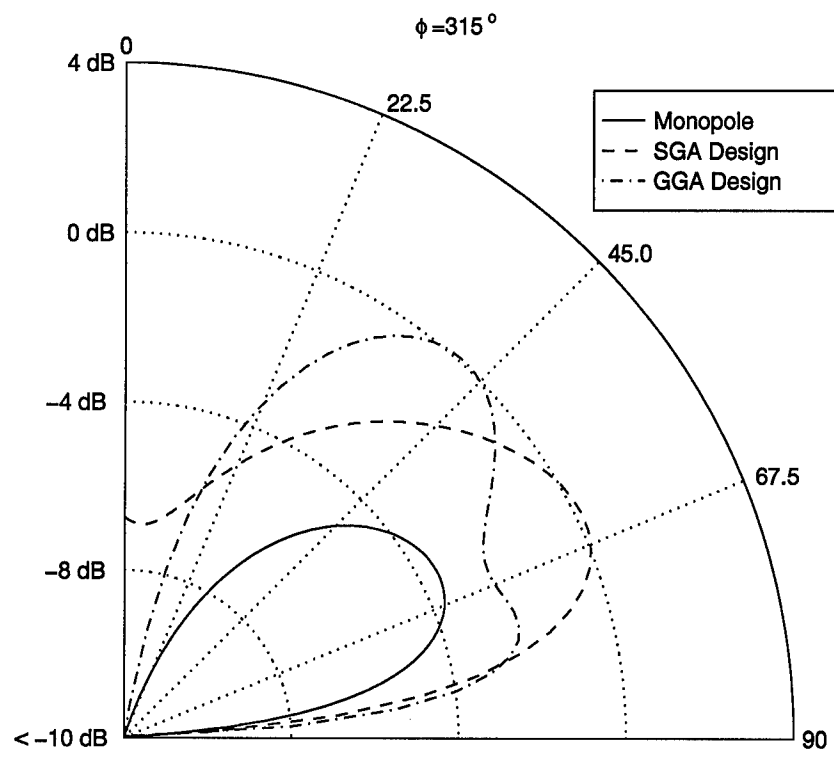
Figure 4.11   Four-Wire Geometry: Elevation Cut of Power Gain at an Azimuth of $\phi = 315°$

In terms of total power gain, the GGA design is clearly superior to the RIMS monopole over all azimuth and zenith angles, yet the power gain calculation takes into account both the horizontal and vertical fields. The question remains, can a receive antenna take advantage of this gain? To answer this question, polarity must be addressed.

4.2.3 Polarity. This analysis of the polarization mismatch will be restricted to the $\theta = 90°$ plane, focusing totally on the use of these antennas on the surface. To conduct the analysis, I define the *observation angle* and the *receiver orientation angle*, which are illustrated in Figure 4.12. The transmitting and receiving antenna coordinate systems are defined in primed and unprimed coordinates, respectively, and correlate to the same coordinates used to display the antenna geometries in Figures 4.2 and 4.3. The observation angle refers to the angle at which the transmitting antenna is being observed, while the receiver orientation angle describes the positioning of the receiving antenna with respect to the line between the two antennas. Elevation is not a consideration, since RIMS components are used on the surface—all antennas will be located on the flat surface assumed in Section 1.6.2.
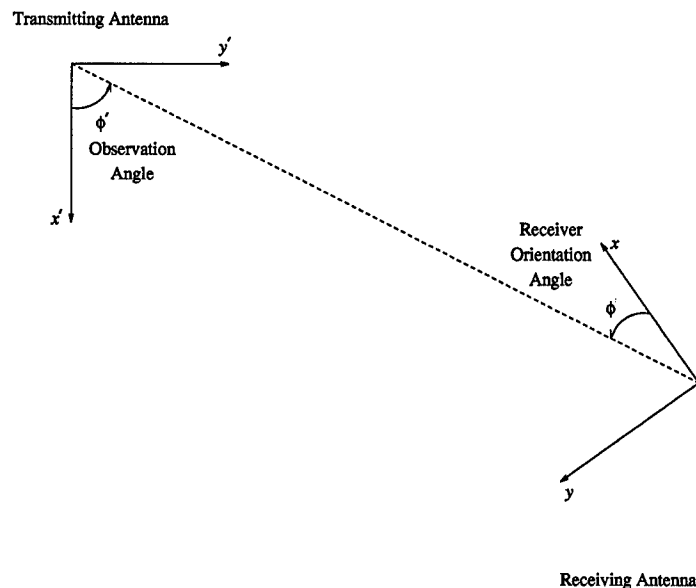

Figure 4.12   **Definition of Angles Used to Determine Loss Due to Polarization Mismatch**

4-15

One can look at the antenna geometries shown in Figures 4.2 and 4.3 and intuitively determine that the radiated waves from these antennas will be elliptically polarized. Because the GGA design's geometry has a more vertical nature, one might speculate that its fields are more vertically oriented than those of the SGA design. This hypothesis is supported in the following analysis.

First, consider the situation where the genetic antennas are the transmitting component of a two-way communication system. If the receiver of the system is the typical RIMS verticle monopole, then the calculation of the losses due to polarization mismatch for each of the genetically-designed transmitters are presented in Figures 4.13 and 4.14.

Figure 4.13   Loss Due to Polarization Mismatch with a Vertical Monopole as the Receiver and the SGA Design as the Transmitter Computed in 2° Increments

In the case of the SGA design, a large amount of loss is experienced when the receiver is vertically polarized. The best-case loss for this system is -0.15 dB, which occurs at an observation angle of 190°. The worst-case loss of -20.15 dB occurs at 106°. In this case, if

4-16

the antenna observation angle is considered to be a uniformly distributed random number, the probability that the polarization loss will exceed -3 dB is 58.9%. From Equation 3.39 and not considering other losses, a loss of -3 dB translates to a range degradation of *at least* 29.3%, which is clearly undesirable.
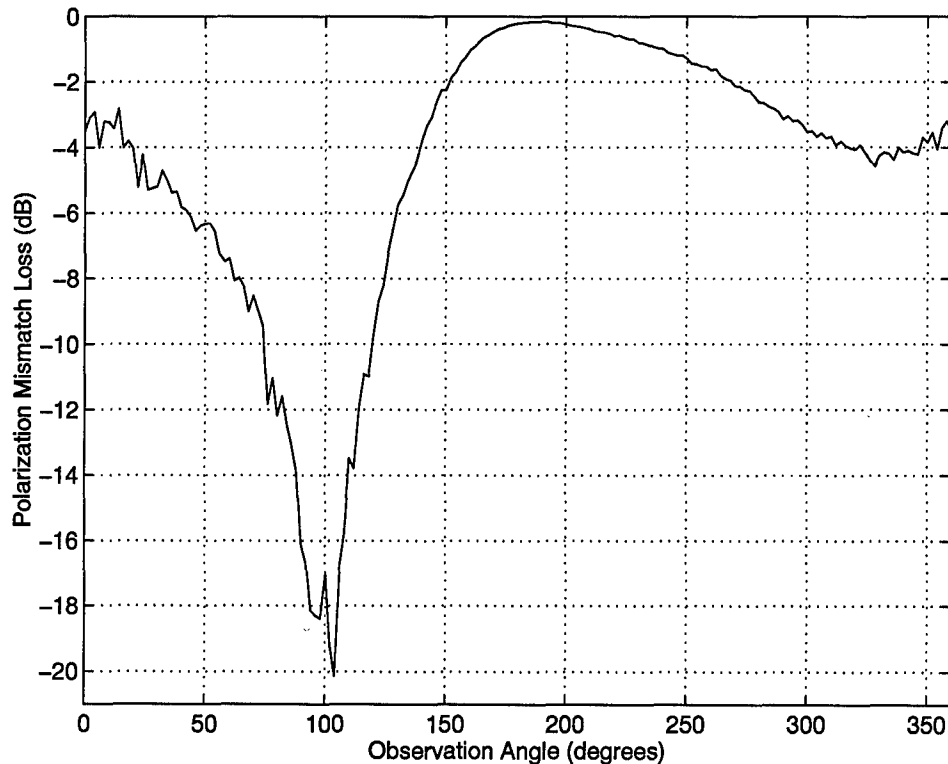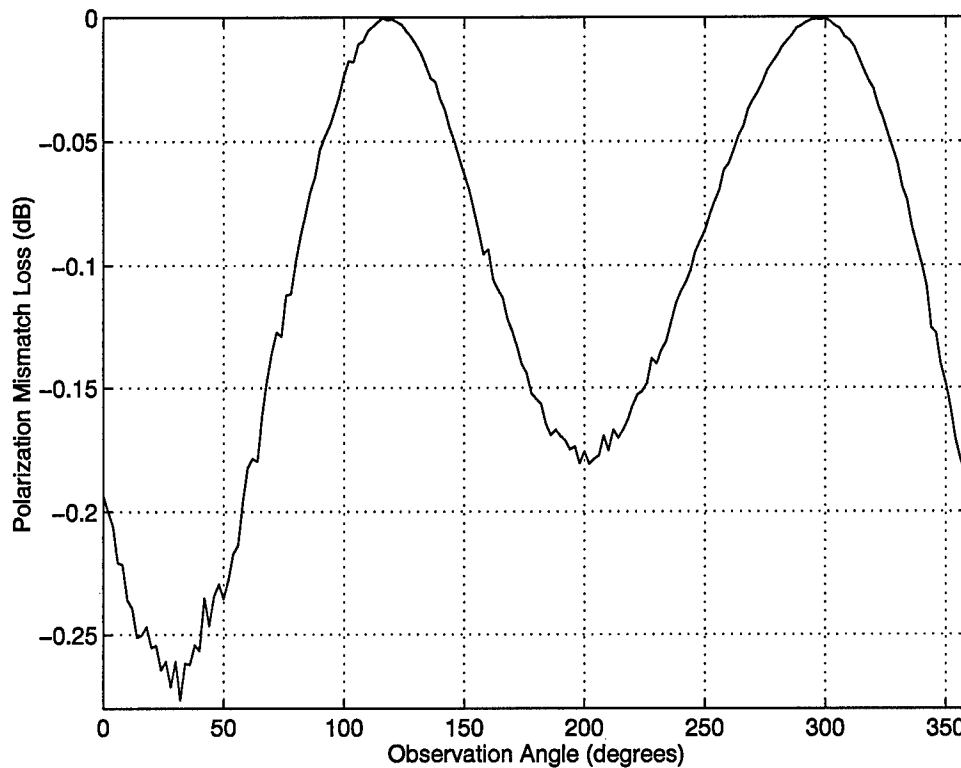

Figure 4.14   **Loss Due to Polarization Mismatch with a Vertical Monopole as the Receiver and the GGA Design as the Transmitter Computed in 2° Increments**

The GGA proves to be the very best case possible because the greatest amount of loss the system could suffer is -0.26 dB, which occurs when the receive monopole is located near $\phi = 30°$. This smaller loss equates to a range degradation of a mere 2.9%. Clearly, the wave radiated by the GGA design is more compatible with a vertical monopole antenna than the SGA design.

What if the receiving unit is not a vertical antenna but one of the GA designs? One would be expect the polarity losses to be larger for this situation, since the GA designs radiate elliptically polarized waves. In the situation that the SGA design is used at both ends and the
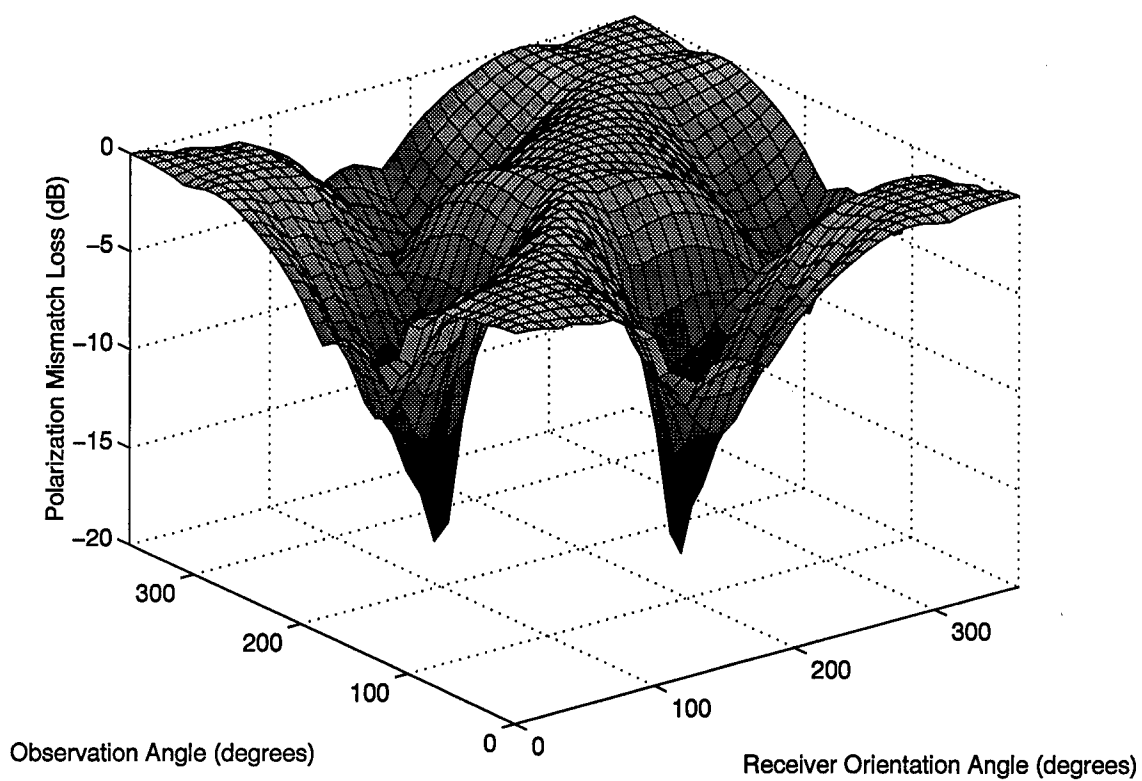
4-17

Figure 4.15   Loss Due to Polarization Mismatch with the SGA Design as the Receiver and Transmitter (Opposite-Sense Polarity) Computed in 10° Increments

receiver has an opposite-sense polarity (constructed in a manner identical to Figure 4.2, the result of Figure 4.15 is seen. In this case, the losses are again large, with a worst-case loss of -16.8 dB. Contrary to the hypothesis that this loss would be larger than the loss experienced with the vertical antenna as a receiver, this loss calculation is not greater in magnitude, which is explained by the fact that the polarization mismatch loss of Figure 4.15 was computed in 10° increments as opposed to 2° increments in Figure 4.13, so some values of loss could have been missed by the discrete computation. This phenomena could also be explained by the fact that the vertical antenna does not have the capability to receive the horizontally polarized component of the transmitted field, while the SGA design has such an ability.

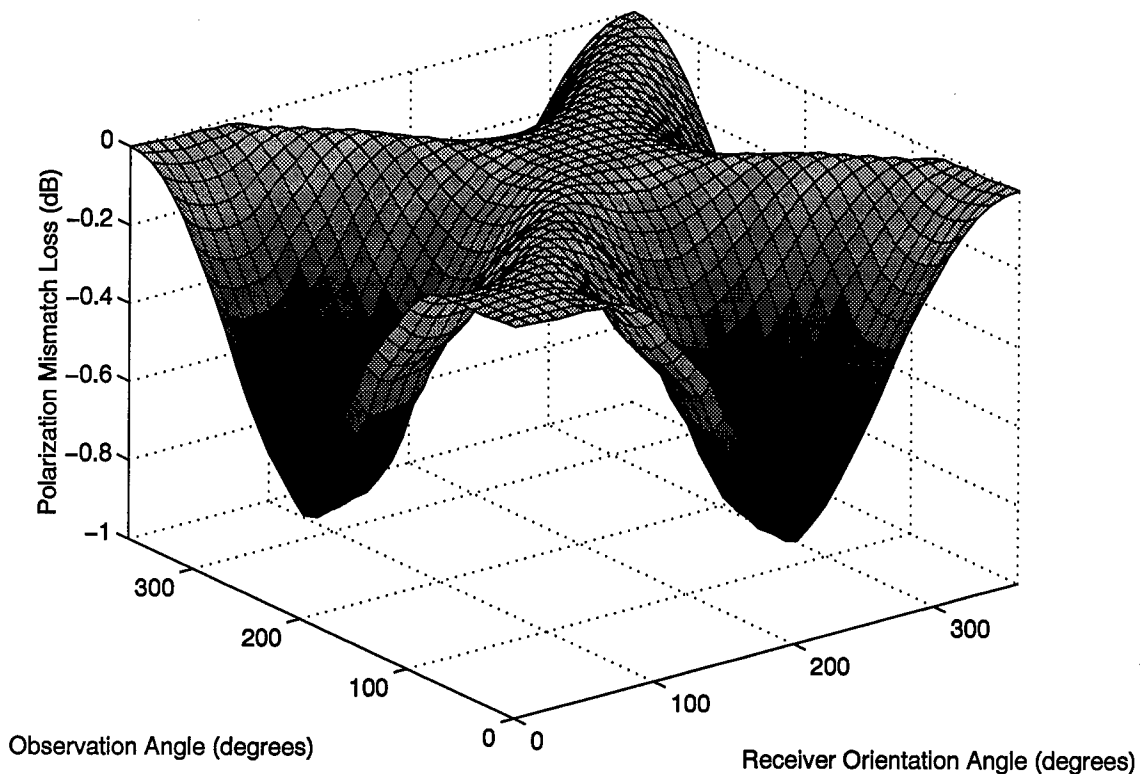Figure 4.16   **Loss Due to Polarization Mismatch with the GGA Design as the Receiver and Transmitter (Opposite-Sense Polarity) Computed in 10° Increments**

For the opposite-sense polarity case where the GGA is at both ends of the link the polarization mismatch loss of Figure 4.16 occurs. In this case, up to -0.77 dB loss could be experienced. As expected, the worst-case loss exceeds that for the linear-receiver case, but

4-19

the loss is still profoundly better than the SGA case and can be attributed to the GGA design's less elliptical and more linear radiated fields.

Figure 4.17   Loss Due to Polarization Mismatch with the SGA Design as the Receiver (Same-Sense Polarity) and the Transmitter Computed in 10° Increments

If the receive antenna is constructed in a fashion as to achieve same-sense polarity, the polarization losses for using the genetic antennas at both ends of the link are shown in Figures 4.17 and 4.18. The elliptical nature of the SGA design is again evident by high losses due to polarity mismatch. Note that for the GGA design, there are still some positions of high loss, up to -0.83 dB, and increased amounts of loss when both angles are close to 0°.

Notice how the loss with a same-sense polarity GGA receiver of Figure 4.18 is not as flat as that of the opposite-sense polarity receiver in Figure 4.16. This is an interesting result and indicates that if the GGA design were to be used at both ends of a communication system, no need would exist for separate construction of the geometries for the recieve and transmit antennas.
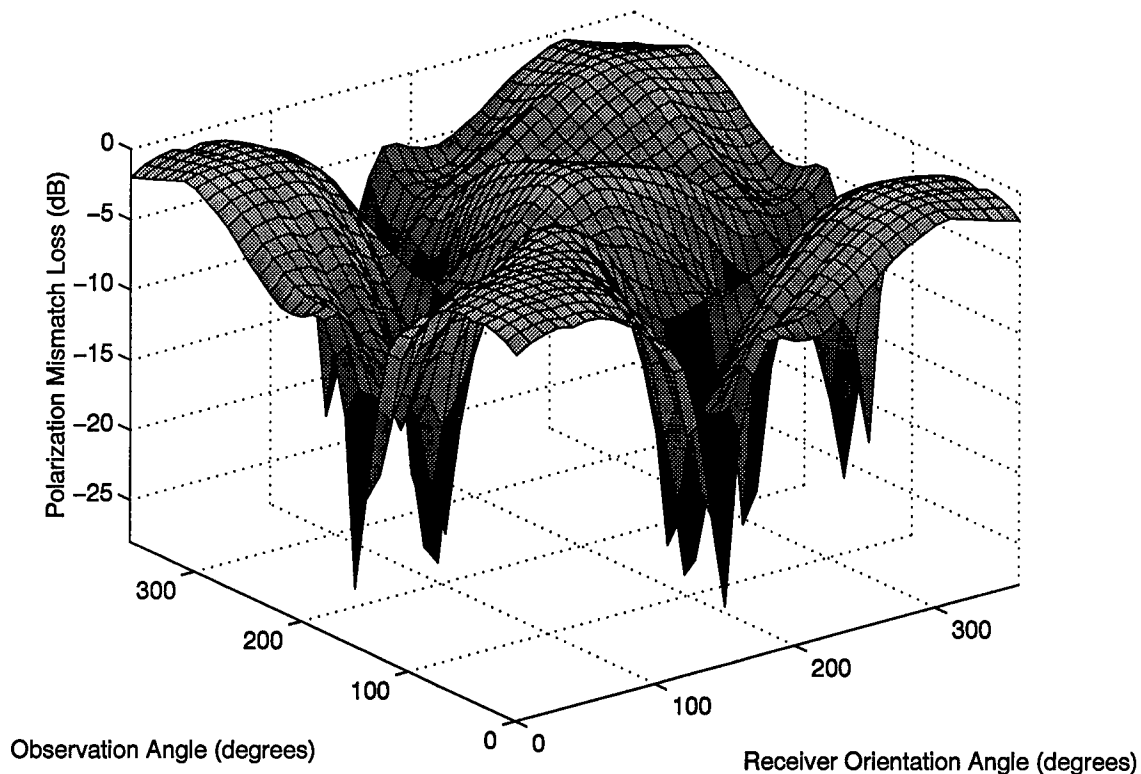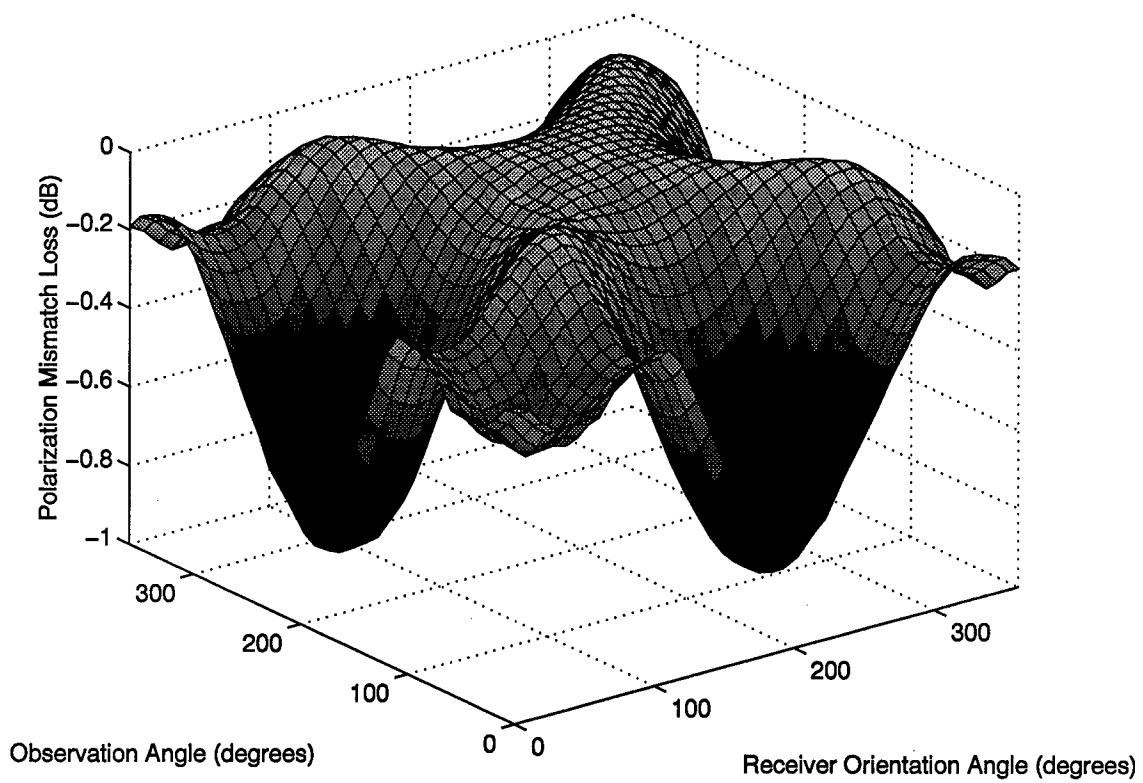
Figure 4.18   Loss Due to Polarization Mismatch with the GGA Design as the Receiver (Same-Sense Polarity) and the Transmitter Computed in 10° Increments
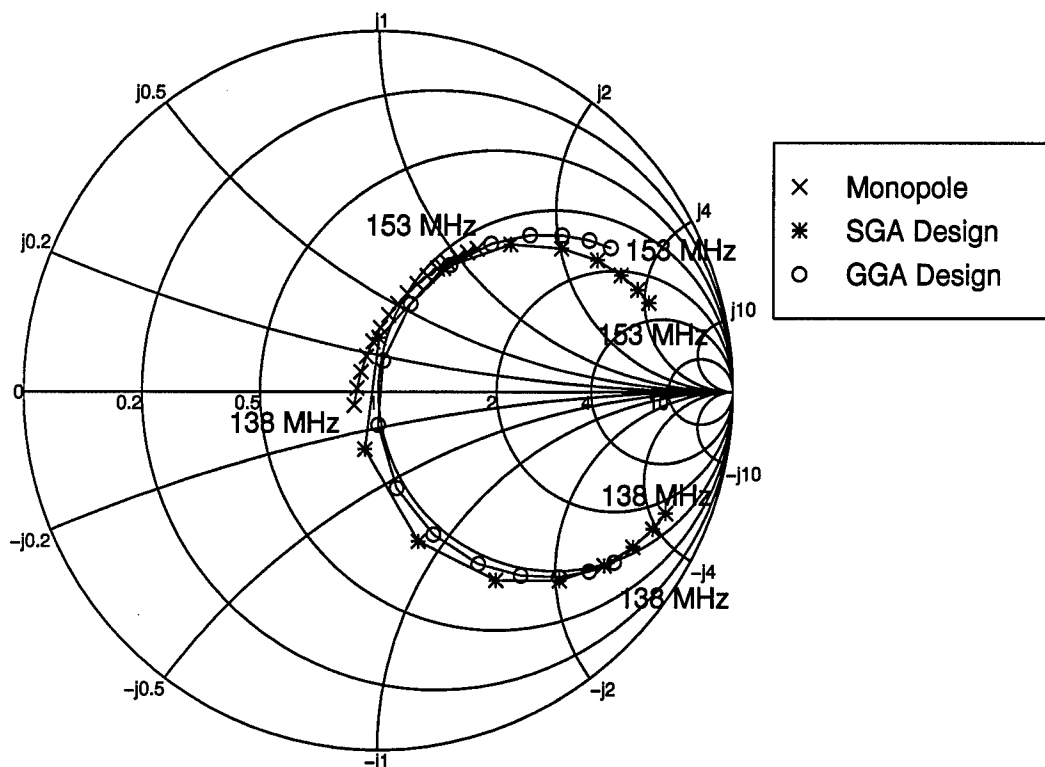
Figure 4.19   **Input Impedance of the GA Designs vs. a Typical RIMS Monopole**

4.2.4   Input Impedance.   It is clear from the Smith Chart of Figure 4.19 that
the four-wire antenna designed by GGA has a far superior impedance match at the center
frequency than the monopole. The SGA design is less well matched than the GGA design but
is still better than the monopole at the center frequency. When moving away from the center
frequency, however, the reactance of both designs becomes very large. Results such as these
in preliminary research led to the expanded problem description of the wire tree antenna to
introduce more coupling between the wires of the design.

From Figure 4.19, the impedance over the frequency band correlates to an impedance
mismatch loss of at most -6.4 dB for the SGA design and -4.8 dB for the GGA design.
However, at the design frequency of 145.5 MHz, both GA designs experience very little loss
because they are well matched. The losses experienced at other frequencies could easily be

overcome with a simple matching network, but an investigation of such a network is beyond the scope of this research.
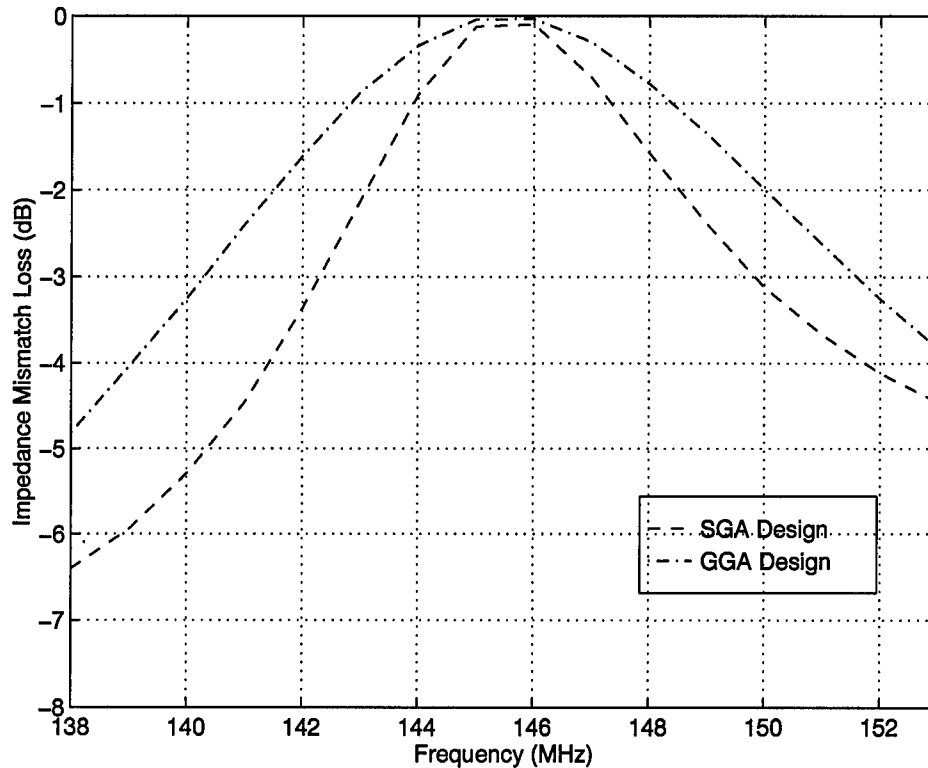
Figure 4.20   Loss Due to Impedance Mismatch for the GA Designs

4.2.5 Improvement.   Considering the worst-case losses at 145.5 MHz, the improvement as computed by Equation 3.42 for the GGA design is shown in Figure 4.21. The SGA is not shown in Figure 4.21 because the losses due to polarization mismatch are too great for any improvement to be experienced. The maximum value of range improvement is 2.70, and the minimum is 1.54. Thus, the GGA design is guaranteed to provide a 54% improvement in range when used at the earth's surface.

4.3   Extended Geometry Results

With the geometry constraints defined, trials were established to determine the best antenna possible for a total number of wires in the wire-tree. The research intended to keep

Figure 4.21   Range Improvement over the λ/4 Monopole Obtained by Using the GGA Design as the Transmitter and Receiver at 145.5 MHz

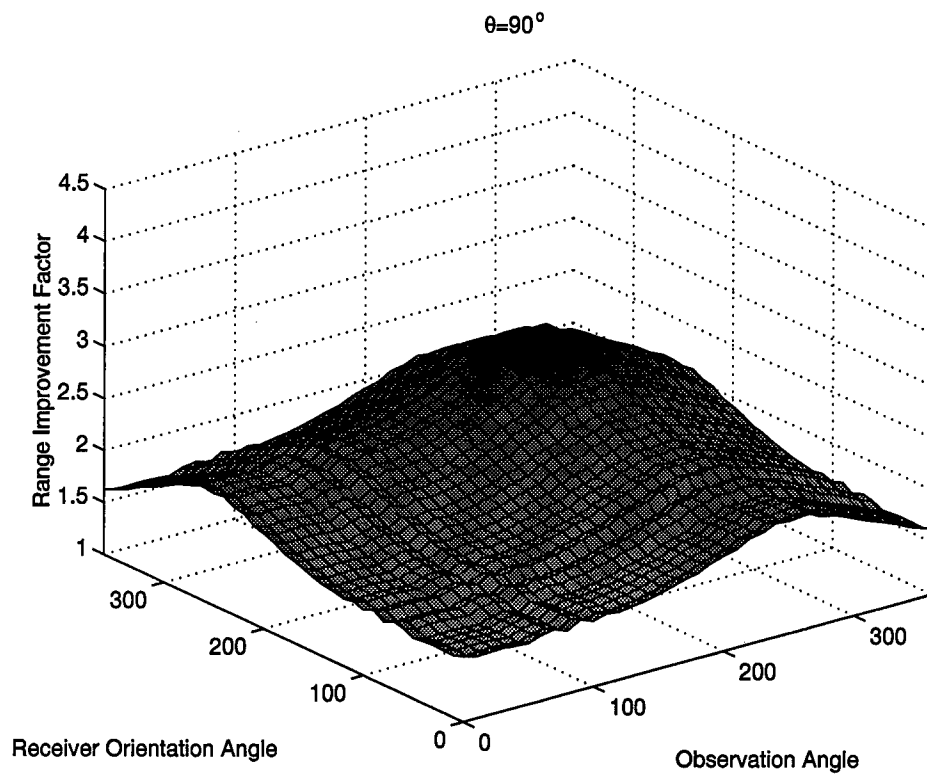| Run #	Fitness						
	3 Wires		4 Wires		5 Wires		
	M=3, B=0	*M=2, B=1*	*M=4, B=0*	*M=2, B=2*	*M=5, B=0*	*M=3, B=1*	*M=2, B=3*
1	75.6	70.1	70.1	73.4	72.3	75.3	72.2
2	78.4	73.0	70.1	73.1	73.2	74.0	71.0
3	74.8	70.0	70.1	71.1	73.1	73.8	70.0

Table 4.2 **Trial Matrix for Finding the Optimal Antenna Given the Extended Geometry Constraints**

the number of wires small to ease in the implementation of such an antenna design. Too many wires in the design would seem cumbersome and would increase the complexity of manufacture. The trials explore all combinations of the wire-tree geometry given that the total number of wires in the structure is three, four or five. The trial matrix is shown in Table 4.2. The geometry definition allows for a more direct comparison of series-connected geometries to the wire-tree geometries.

For this expanded problem definition, the antenna with the best fitness out of the runs of Table 4.2 was not an antenna that incorporated branching. Since the concept of the series design is not new, and none of the runs of Table 4.2 produced a fitness greater than that of the GGA design, the resulting antennas are not analyzed further.

4.4 Symmetrical Geometry Results

The GGA design performance left some performance characteristics to be desired. Although the power gain at low elevation angles is better than the monopole, it is not remarkably better as indicated by its guaranteed range improvement of only 54%. Symmetry in the GGA design's radiation characteristics was also a factor as noted by its uneven range improvement in Figure 4.21. Early research did not indicate much benefit from symmetrical designs (44:310–311). Despite the early research, the results of the GGA design analysis led to the creation of the VLM geometry definition. With the new geometry of Figure 3.6, the SGA was used for optimization.

The resulting optimized version of the VLM antenna is shown in Figure 4.22 and is notable because of its 1.293 meter vertical wire appended by four 1.162 meter long loading wires, which come very close to but do not touch the ground.
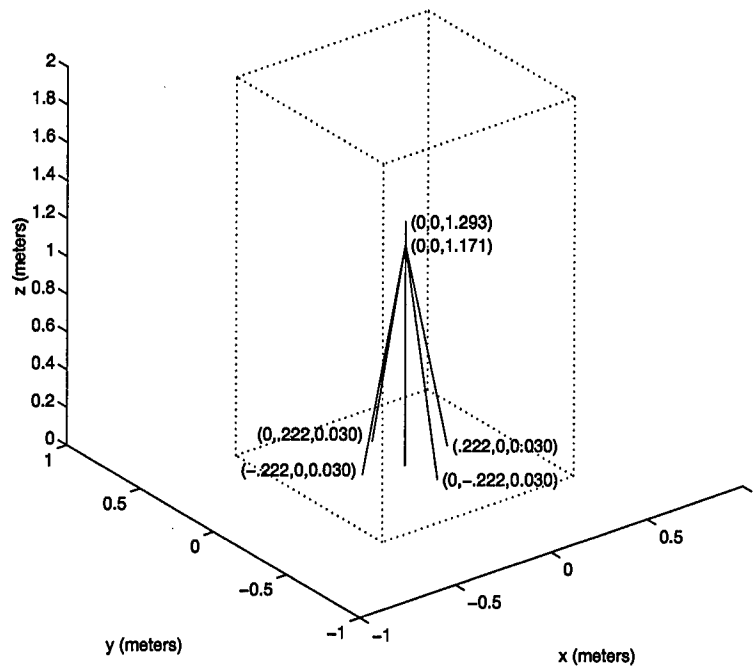
Figure 4.22 **Symmetrical Wire Antenna Geometry Optimized Using the SGA**

Another point of note is that the VLM geometry was optimized using finitely-conducting wires made of copper ($\sigma = 5.8 \times 10^7\ \mho/m$). In NEC4.1, these wires are modeled as a distributed load (40:60–62). The modeling of realistic wires causes the optimized geometry to overcome the loss in the wires for impedance matching purposes, as well as producing more realistic gain figures.

4.4.1 Power Gain. The VLM design displays a significant improvement in power gain over the vertical monopole and the GA designs previously analyzed. The VLM has good gain over the earth surface as shown in Figures 4.23 and 4.24.
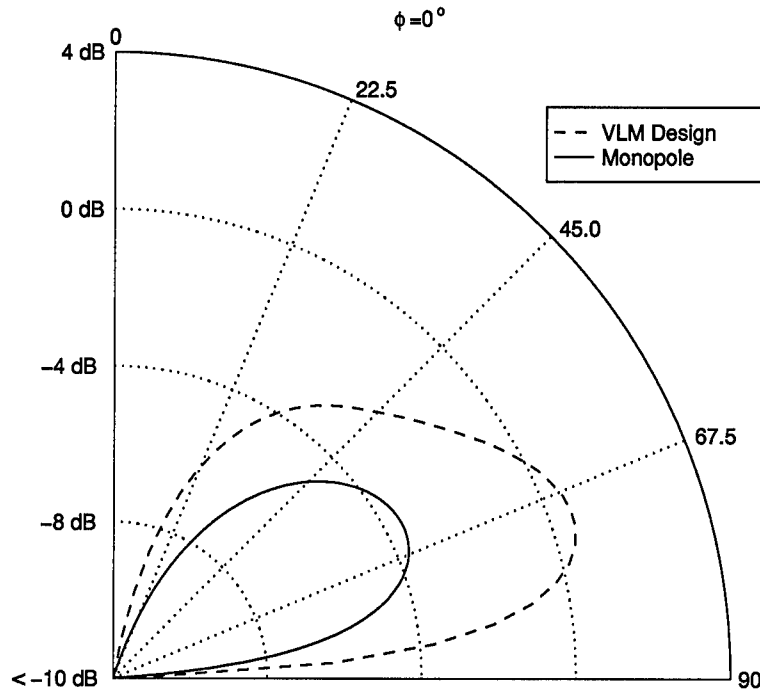
Figure 4.23 VLM Geometry: Elevation Cut of Power Gain at an Azimuth of ϕ=0

The correlation between the $\phi = 0°$ and $\phi = 45°$ elevation cuts is good, giving a strong indication of the benefit obtained by imposing symmetry on the design. In each of the elevation cuts of Figures 4.23 and 4.24, at $\theta = 67.5°$ the VLM design surpasses the monopole by over 4 dB. This amount increases to nearly 8 dB at $\theta = 80°$. This improvement in space-wave gain is highly desirable and will benefit the RIMS user.

Due to the symmetry of the VLM design, no additional elevation cuts are required for a complete understanding of the gain.

4.4.2 Polarity.   The biggest advantage with the VLM design is that the radiated fields are almost entirely linear or elliptical with axial ratios on the order of 10^{-4}. Thus, the loss due to polarization mismatch when the VLM is used as the receiver for a VLM transmitter is negligible, as is evident in Figure 4.25.

4-27

Figure 4.24   VLM Geometry: Elevation Cut of Power Gain at an Azimuth of ϕ=45
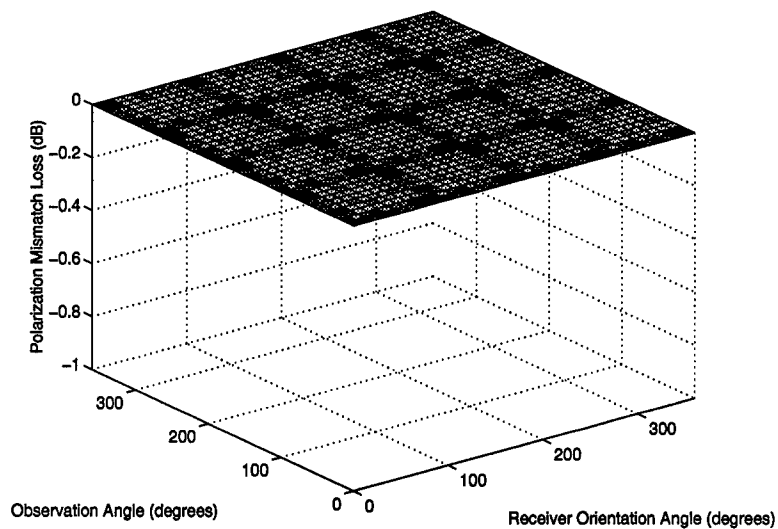
Figure 4.25   Loss Due to Polarization Mismatch with the VLM Design as Both Receiver and Transmitter

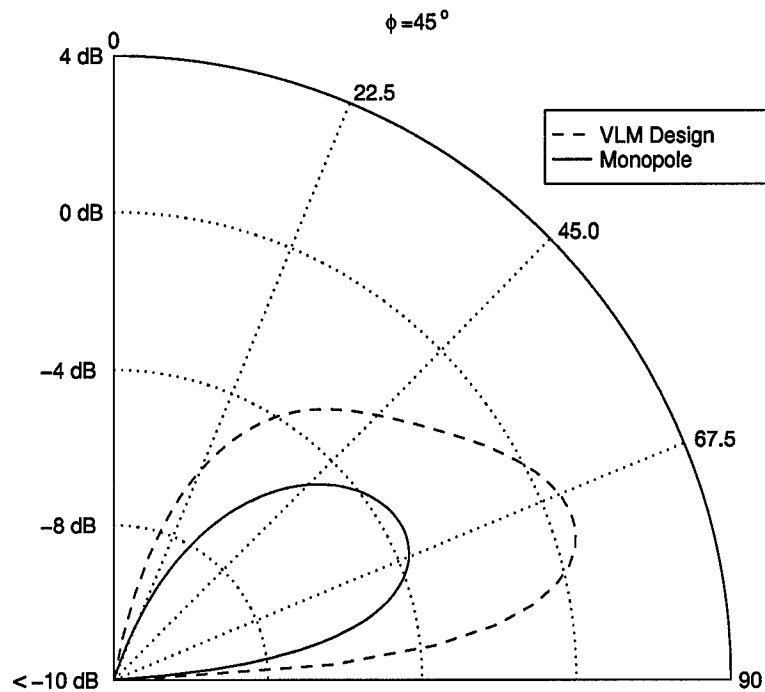*4.4.3 Input Impedance.* The impedance equates to impedance mismatch losses of no more than -2.3 dB from Figure 4.26, 2.5 dB better than that of the GGA design. The explanation for this result is that the VLM design approximates the geometry of a cone, which is well known for its wideband characteristics (45:464). The better frequency response implies that the implementation of a matching network would be much easier for the VLM antenna than the GGA design.
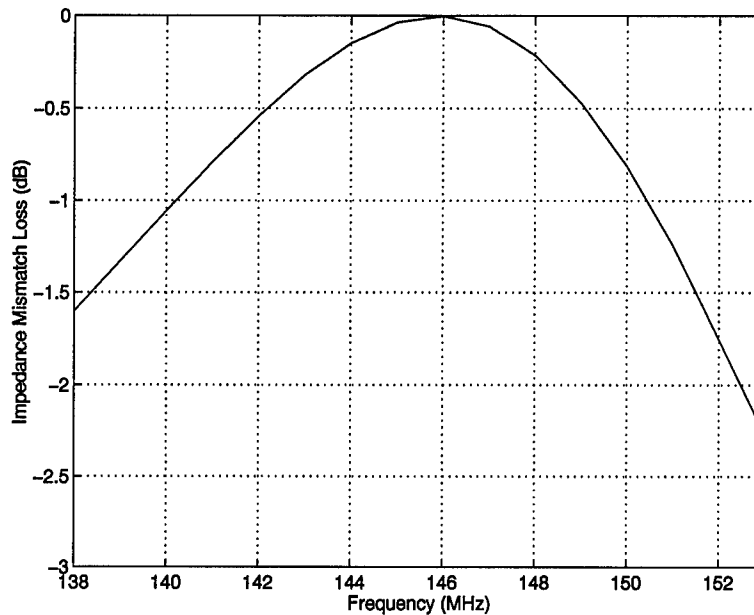
Figure 4.26   **Loss Due to Impedance Mismatch for the VLM Design**

4.4.4 Improvement. The VLM provides a significant improvement over the monopole, as witnessed in Figure 4.27. Note that while the GGA design can only guarantee a 54% increase in range, VLM design offers a whopping 252% increase in range at 145.5 MHz, with a minimum κ of 3.52, attainable because the losses due to polarity and impedance mismatch are insignificant.

4.4.5 Current Distribution. A study of the current provides a good qualitative check into the reasonableness of the MoM solution for the antenna. Figure 4.28 shows the magnitude of the current as a function of position on the wires of the antenna. First, note

4-29
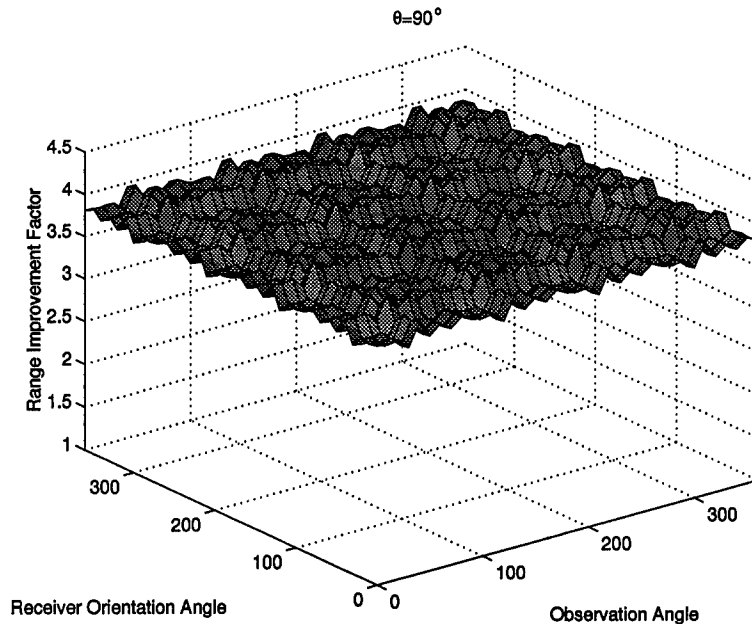
Figure 4.27   Range Improvement over the λ/4 Monopole Obtained by Using the VLM Design as the Transmitter and Receiver at 145.5 MHz

that the current plotted is that of the current in the center of each segment used in the MoM computation, which explains why the current magnitude does not diminish to exactly zero at the ends. Another important check is that the current magnitude is continuous at the junction, noted in the figure with a dotted line. At first glance, it would appear that the current magnitude is not continuous over the junction, as indicated by the discontinuity along the vertical wire. However, if the magnitude of the current at the beginning (position=0) of each of the four loading wires is taken to account at the junction, the current magnitude becomes continuous.

The effect of mutual coupling between wires is evident in two places. The first is at the junction, where the current magnitude peaks to a maximum value due to the density of these wires. Second, the shifting of the small null in the current magnitude along the loading wires shows coupling. Backing up from the end of the loading wires, at the frequency of 145.5 MHz, one would expect the null near the 0.65 meter position. Also, notice how the current nulls do not reach zero in the middle of the wires, another detail attributed to the coupling effect.

4-30
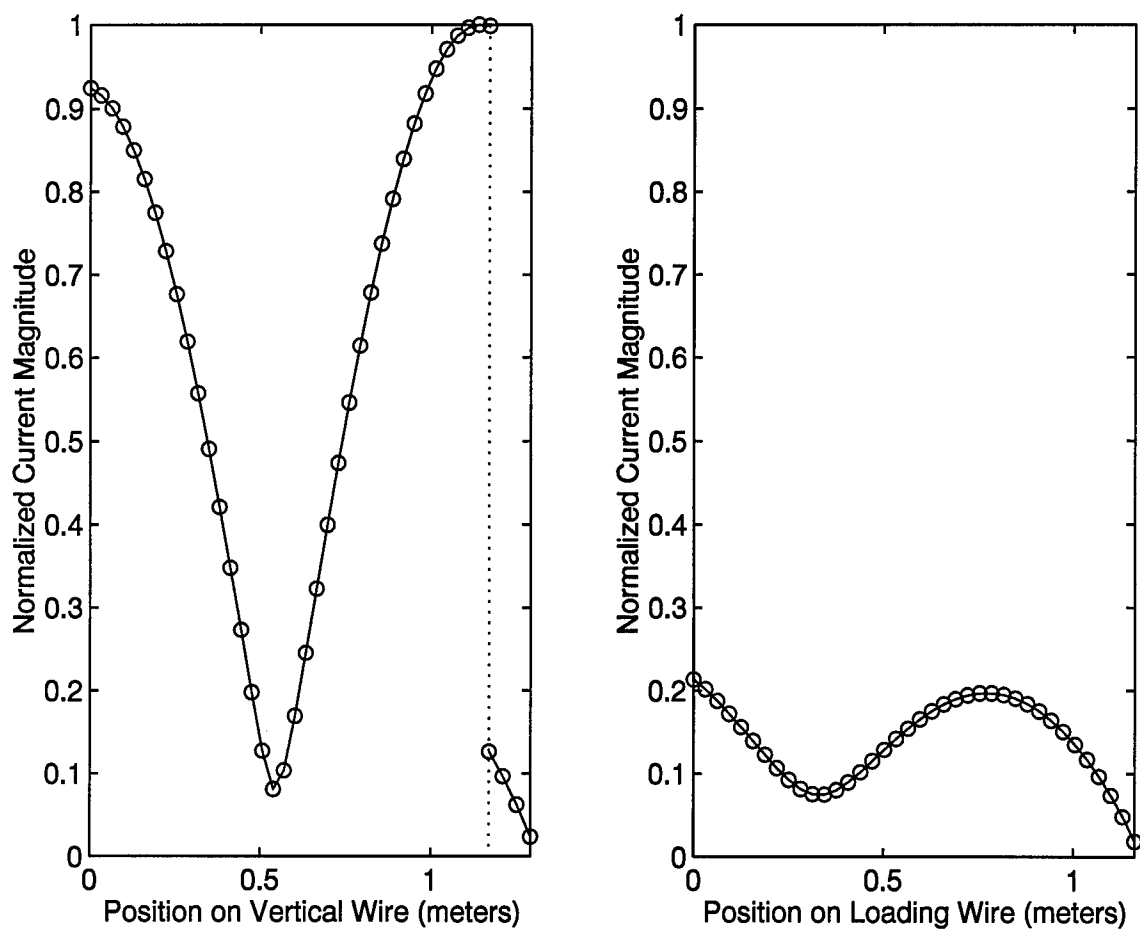
Figure 4.28   Currents on the VLM with the Wire Junction Designated by the Dotted Line

4.4.6 Frequency Characteristics. The analysis of Section 4.4.4 was performed at the center frequency of the band of interest, namely 145.5 MHz. To extend the analysis, the frequencies at each end of the 138.0–153.0 MHz band are considered. The assumption is that the improvement is measured against the monopole operating at the center frequency, which is assumed to be perfectly matched. This assumption provides a worst-case analysis.
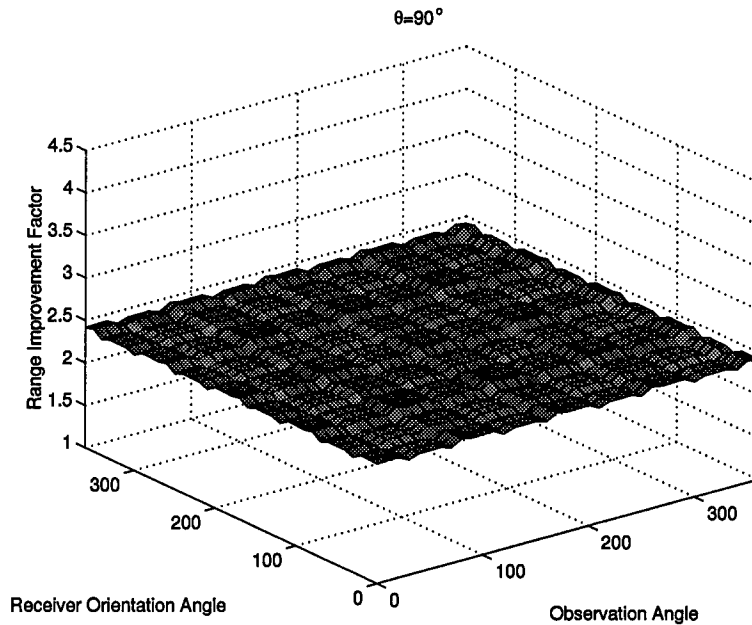
Figure 4.29   **Range Improvement Factor Computed at 138.0 MHz Including All Losses**

When operating at 138.0 MHz, the VLM suffers negligible polarization mismatch loss, which is expected since polarization is mainly a function of antenna geometry. However, the impedance mismatch loss will be significant when exciting the antenna at different frequencies. In the case of 138.0 MHz excitation, -1.60 dB of loss from Figure 4.26 is attributed to impedance mismatch, which has a profound effect on the range improvement shown in Figure 4.29. The minimum value of κ in this case is 2.28, corresponding to a range increase of only 128%, a considerable degradation from that achieved at the center frequency but still a large improvement over the monopole. Similarly, at 153.0 MHz, the range increase is degraded further, down to 122%, as can be determined from Figure 4.30.
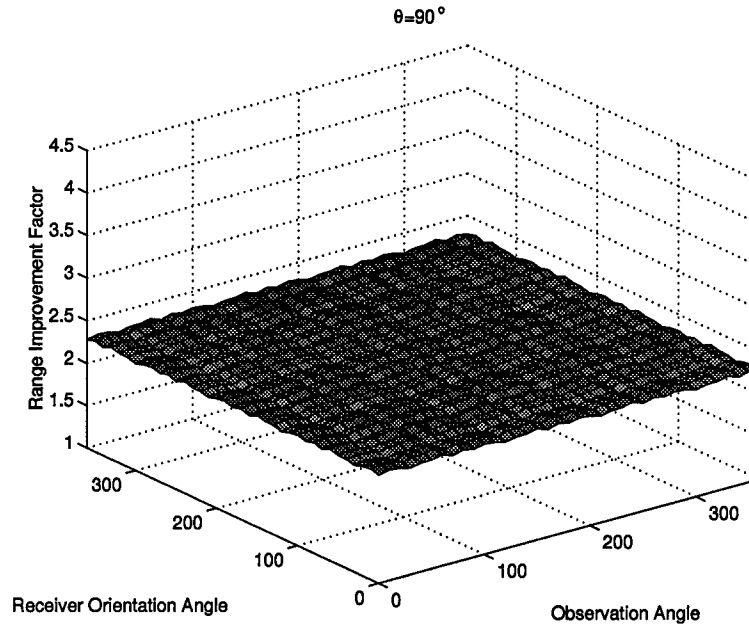
Figure 4.30   Range Improvement Factor Computed at 153.0 MHz Including All Losses

The important point to mention in this frequency analysis is not that the range improvement is degraded, but that the polarity of the antenna is not affected over the band. The loss due to matching can be easily overcome with a matching network that provides sufficient performance over the entire band. Even if such a matching network is not implemented, the range improvement is significant.

4.4.7   Effect of Different Soils.   It is important to understand how the antenna will perform under different types of conditions. The soil used for optimization bordered on the region between dielectric and quasi-conducting soil (43:548). Using the same soils used in Section 4.1.2, the range improvement factor is re-derived for these two conditions. The results are shown in Figures 4.31 and 4.32.

The result is that for a the dielectric ground, the range improvement is degraded from Figure 4.27's minimum value of 3.52 with a minimum κ of 3.10. For the quasi-conducting ground, the minimum κ drops further to 2.37. The explanation for this is simple based on the

θ=90°
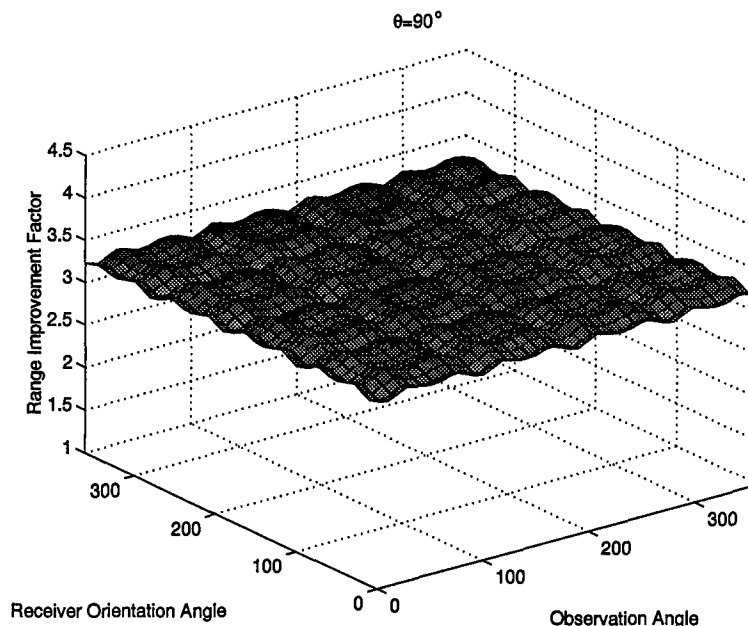
Figure 4.31   **Range Improvement Factor Computed at 145.5 MHz Over Dielectric Ground Including All Losses**

method by which the range improvement factor is formulated. In the extreme cases of ground type, the difference between the monopole and the VLM becomes less pronounced.

By examining different grounds, it is shown that performance of the VLM antenna varies over the different types of ground but will always show improvement over the monopole. This result is important because the geometry was optimized for a specific type of ground. However, by picking a ground along the boundary between dielectrics and quasi-conductors, acceptable performance was obtained in both regions.

4.4.8   Geometry Sensitivity.   The VLM design will not be of much practical use if the geometry points prove to be intolerant of some variance. If the manufacturing tolerance requires the geometry to be accurate to the nearest millimeter, the antenna will not serve well in an operational environment in which the geometry may be altered.

To study the sensitivity of the design, zero-mean Gaussian geometry errors were added to the coordinates of the design, the only stipulation being that the first wire still begins at

4-34
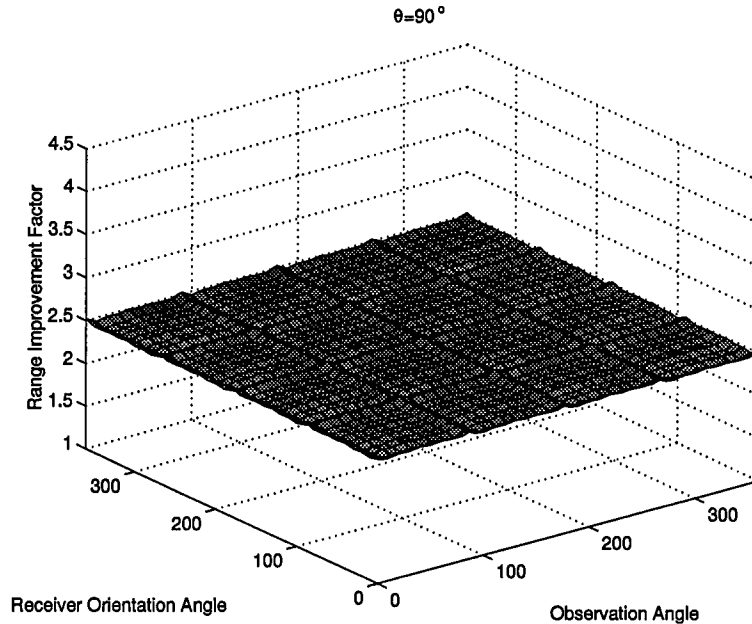
Figure 4.32   **Range Improvement Factor Computed at 145.5 MHz Over Quasi-Conducting Ground Including All Losses**

$(0, 0, 0)$ and the four loading wires are all affixed to the same location, which are reasonable assumptions given practical considerations.

Figure 4.33 shows the resulting range improvement factor for the VLM whose coordinates are shifted by noise with a variance of 1 cm. The minimum value of κ in this case is 3.69. The noise did not introduce significant losses due to polarization or impedance mismatch. In fact, the minimum κ is better than that of the non-corrupted design.

When the VLM design is changed by random geometry adjustments with a variance of 3.0 cm, the result of Figure 4.34 is obtained. In this case, the minimum κ is 3.57, again better than that of the non-corrupted VLM. In this case, small polarity mismatch losses are introduced on the order of 10^{-3} dB.

For the final case of geometry alterations with a variance of 5.0 cm, the resulting minimum κ from Figure 4.35 is 3.65. Again, polarization mismatch losses of 10^{-3} dB are introduced, while the impedance mismatch remains negligible.

θ=90°

Figure 4.33   Range Improvement Factor Computed at 145.5 MHz for VLM Antenna Corrupted by Zero-Mean Gaussian Geometry Errors with a Variance of 1.0 cm

θ=90°

Figure 4.34   Range Improvement Factor Computed at 145.5 MHz for VLM Antenna Corrupted by Zero-Mean Gaussian Geometry Errors with a Variance of 3.0 cm

θ=90°

Figure 4.35   Range Improvement Factor Computed at 145.5 MHz for VLM Antenna Whos
Geometry is Corrupted by Zero-Mean Gaussian Noise with a Variance of 5.0 cm

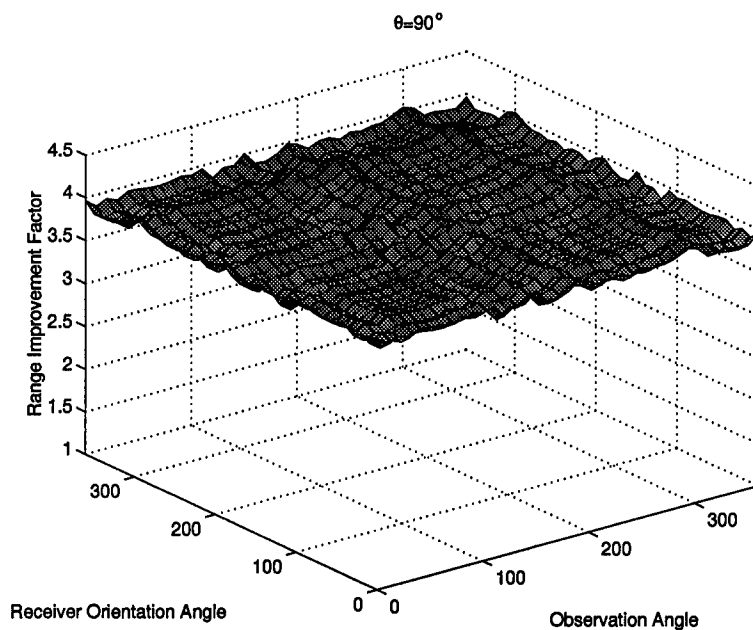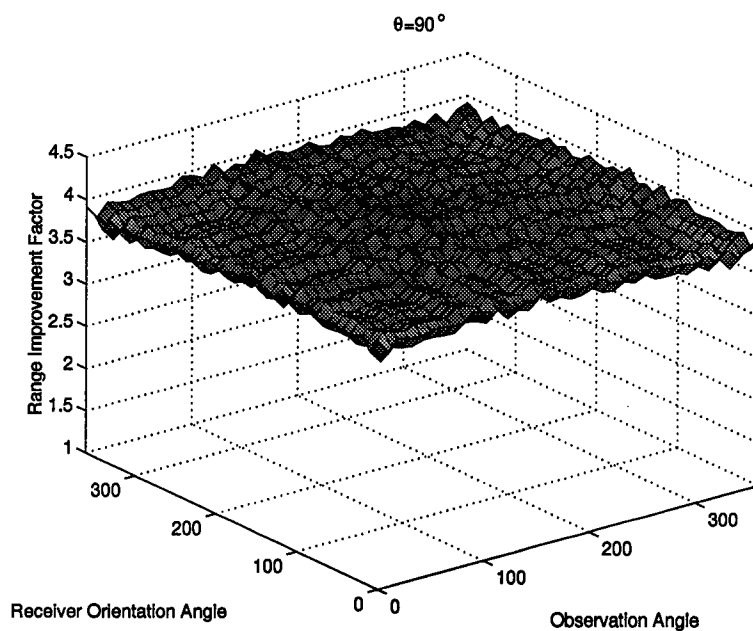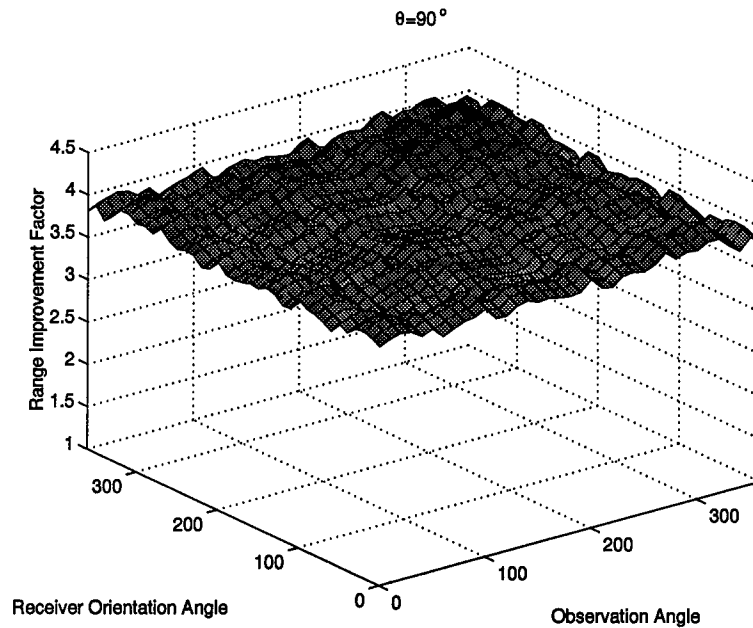This study into geometry sensitivity implies that the VLM antenna is very stable to
large corruptions in its geometry, making it a very practical antenna for the operational
environment.

V. Findings and Conclusions

5.1 Findings

5.1.1 Simple Versus Complex Genetic Algorithms.

As evident in Chapter II, many in the electromagnetics community are using simple genetic algorithms for optimization. The direct comparison in this research effort hopes to show that the elementary GA might not be the most extensive search tool given the availability of sophisticated GA codes from the computer science community.

The more complex GGA algorithm proved to be more capable in both domains. In the GA domain, its variety of crossover and mutation operators made it possible for the GGA to find a wire-geometry with a high fitness not achievable using the SGA. In the antenna domain, the resulting antenna produced a much more desirable antenna because the radiation from the SGA design was not very symmetrical.

5.1.2 Using GAs for Insight.

With fewer restrictions imposed on the wire geometry, analysis of the GA designs provided valuable insight into structures with desired performance characteristics. Domain constraints incorporating this knowledge opened the way for better-performing designs. No other research seems to have incorporated GAs and electromagnetics in this manner.

By analyzing the less-constrained GGA design, valuable insight was obtained into the fundmental geometry characteristics of an antenna that radiates space-wave fields well over the earth. By starting the process again with new geometry constraints, a superior antenna was produced.

5.2 Conclusions

5.2.1 Recommendation.

For a RIMS application, clearly the best antenna to use is the VLM design, based on its large gain over the earth, more-matched input impedance over the ground sensor band, its frequency stability, and its insensitivity to geometry perturbations.

5.2.2 Further Research.

5.2.2.1 Measurement.
The next logical step with the VLM design is to build a prototype for the purpose of measurement. The measurement process can be approached with much confidence, since NEC predictions have correlated well with measurements for wire antennas in the presence of both perfectly conducting ground planes (33:1681–1682) and lossy-earth-model ground planes (16:295–298).

5.2.2.2 Messy GA.
The results visible in this research are quite interesting, yet the basis of this effort, like many similar studies of GA application in electromagnetics, conforms to a very limiting paradigm. The paradigm is that of string size. Implementation of a simple GA requires that the number of features be fixed.

In the wire antenna geometry implementation of this research, the number of wires was specified prior to running any experiment. The research first picked an arbitrary number, four, and allowed the GA to find the best solution given that constraint. Linden and Altshuler prescribed to the same paradigm and performed multiple experiments using between three and eight wires to design their antenna (4:78). This type of process could continue indefinitely. It would be interesting to allow three wire designs to compete with four, five, seven, and N-wire designs in the evolutionary process. Unfortunately, the coding paradigm restricts this.

The main problem introduced when trying to eliminate this paradigm is how to perform crossover in a way that is reasonable. For example, one string could be represented by

$$c_i = (g_1, g_2, ..., g_m) \quad , \tag{5.1}$$

and another by

$$c_j = (g_1, g_2, ..., g_n) \quad . \tag{5.2}$$

When $m = n$, crossover is trivial. When $m \neq n$, crossover operations can easily be performed without regard to the physical nature of the problem, but it becomes unclear how to

produce offspring in a meaningful fashion. Using the aforementioned samples, let $m < n$. To perform crossover, one could transform c_j to m elements. This could be done by truncation or sampling. Another method would be to characterize each feature value and perform the truncation based on that method. Truncation can easily be dealt with, but continually truncating would seem to cause the GA to converge to smaller phenotypes. To avoid this result, crossover would also have to incorporate an *expanded* c_i. This could be performed in any number of ways, but should retain some knowledge of the physical representation of the string.

Probably the best approach to handling this situation would be to use a *messy GA*. Because the messy GA by definition is capable of handling variable length strings, it is more suitable for this type of problem than the simple GA (46:24). The messy GA can handle crossover by avoiding the types of crossover used in simple GAs by introducing *slice* and *cut* operators, which join or truncate strings with a specified probability (46:25).

By using a messy GA, wire antennas with different numbers of wires could compete directly against one another, and separate trials of the GA for specific numbers of wires would not be necessary.

5.2.2.3 Wideband Design. Though no attempt was made in this research effort, a GA could also be used to design a wideband antenna. This could be done simply. Early on in the research effort, some consideration was given to developing a wide-band RIMS antenna that could be excited with a spread-spectrum signal. Neither the researcher nor the sponsor was interested in pursuing such an idea, but a GA could easily optimize such an antenna, which could be used in spread-spectrum applications.

5.2.2.4 Fractal Coding. Fractal geometry is a way to describe an object by the relationships between its components (47:5). Compared to the bulky nature of determin-istic geometry, which defines an object with affine transformations, scalings, rotations, and congruences, fractal geometry representation is much more compact (47:5). A fractal analogy is the representation of the solar system by simply stating the law of gravitation and providing a set of initial condtions. (47:5).

For simple antenna problems, fractal coding schemes have been incorporated into GA optimization, which greatly reduce the cost of coding the designs into strings (48:1692). Particularly in the case of wire antenna design, this is a wide-open field for research.

5.3 Summary

Two genetic algorithms (GAs) were integrated with Numerical Electromagnetics Code Version 4.1 (NEC4.1) and used to design a wire antenna for use in a remote intrusion monitoring system (RIMS). The results of a simple GA were compared to those of the GENOCOP III package, with the expected result that GENOCOP III outperformed the simple GA. Several different wire geometry definitions for an antenna radiating in the presence of the lossy earth were investigated, and the vertical loaded monopole (VLM) geometry proved to be the recommended antenna for use in a RIMS, based on its relatively high gain over the earth, matched impedance, symmetrical radiation pattern, and linearly polarized fields. The VLM antenna was then investigated for performance over different qualities of earth, different frequencies and for errors in its geometry. The extensive analysis showed that the VLM antenna would perform very well in an operational RIMS environment.

Appendix A. Coordinate System

For this research, the standard spherical coordinate system of Figure A.1 is used. In the research, ϕ is often referred to as the azimuth angle, θ as the zenith angle, and ψ as the elevation angle.
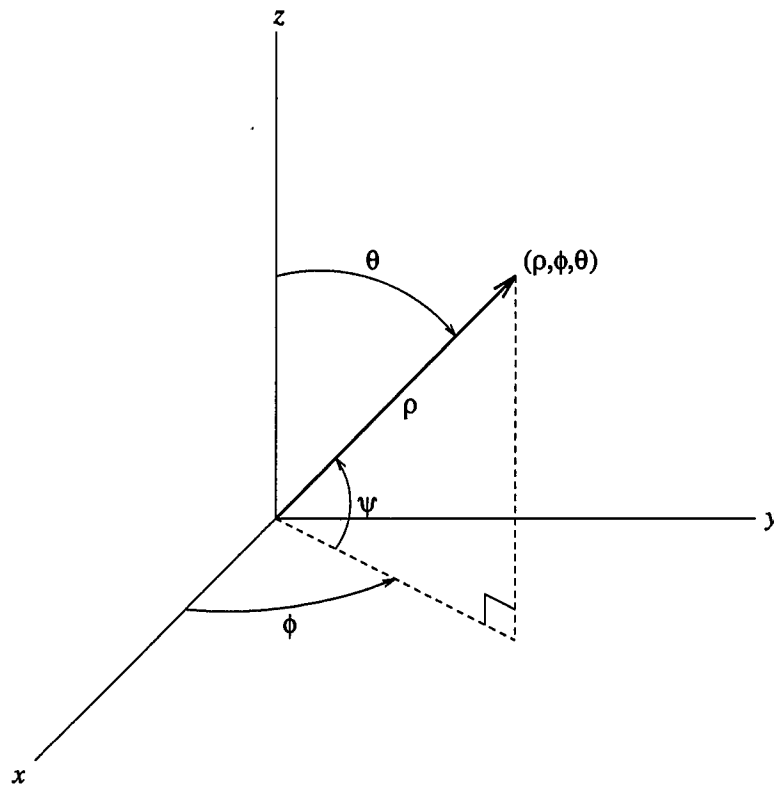
Figure A.1   **Definition of Coordinate System**

Appendix B. Development of Reflection Coefficent for Lossy Ground

This appendix develops the complex reflection coefficents for both polarization cases. This development directly follows the Jordan and Balmain's procedure (12:144–147,629–632).

B.1   Plane Wave Reflection at Oblique Incidence

The first step is to develop the reflection coefficient of an oblique incident wave for two perfect insulators $(\sigma = 0)$ The assumption is that the permeability of both media in Figure B.1 is that of free space, μ_o. Also, it is assumed that the interface is perfectly planar. These assumptions translate to the approximations that it can be applied to the earth/air boundary and applies to locally planar regions of the earths surface, following the assumptions of Chapter I.
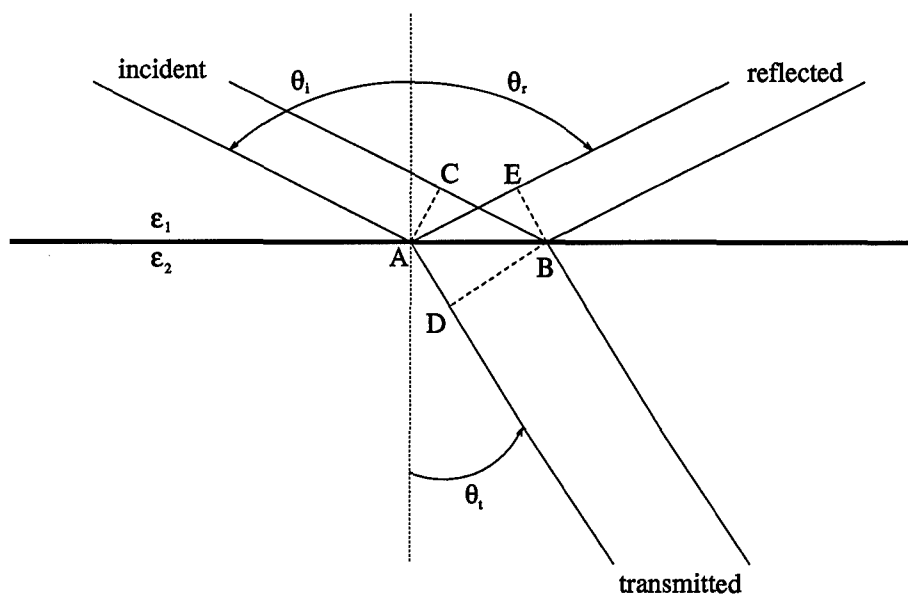
Figure B.1   Plane Wave Reflection at Oblique Incidence With Two Perfect Insulators

Looking at Figure B.1, it is easy to determine that the plane wave will have equal phase along segments AC and BD, leading to

$$\frac{CB}{AD} = \frac{v_1}{v_2} \quad , \tag{B.1}$$

with the velocity in each medium, v_1 and v_2 being defined by

$$v_{1,2} = \frac{1}{\sqrt{\mu_o \epsilon_{1,2}}} \quad . \tag{B.2}$$

From this, one can derive that

$$\frac{\sin \theta_i}{\sin \theta_t} = \sqrt{\frac{\epsilon_1}{\epsilon_2}} \quad . \tag{B.3}$$

Using a similar method, one can also show that

$$\theta_i = \theta_r \quad . \tag{B.4}$$

Recalling that the instantaneous Poynting Vector is

$$\mathbf{P} = \mathbf{E} \times \mathbf{H} \quad , \tag{B.5}$$

one then can look at the magnitude of the average Poynting vector, which is

$$|P_{ave}| = \frac{1}{2} |E|^2 \operatorname{Re} \left\{ \frac{1}{\eta} \right\} \quad . \tag{B.6}$$

Then, using the conservation of energy, form the equation

$$\frac{1}{v_1} |E_i|^2 \cos \theta_i = \frac{1}{v_1} |E_r|^2 \cos \theta_i + \frac{1}{v_2} |E_t|^2 \cos \theta_t \quad . \tag{B.7}$$

From this,

$$\frac{|E_r|^2}{|E_t|^2} = 1 - \frac{\sqrt{\epsilon_2} |E_t|^2 \cos \theta_t}{\sqrt{\epsilon_1} |E_i|^2 \cos \theta_i} \tag{B.8}$$

B-2

is derived. Applying the boundary condition that the tangential component of $\mathbf{E}$ must be continuous across the boundary gives for horizontal polarization

$$|E_i| \cos \theta_i + |E_r| \cos \theta_i = |E_t| \cos \theta_t \quad , \tag{B.9}$$

and for vertical polarization

$$|E_i| + |E_r| = |E_t| \quad . \tag{B.10}$$

Using Equations B.9 and B.10 with the result of Equation B.8, the reflection coefficients are obtained. For horizontal polarization

$$\frac{|E_r|}{|E_i|} = \frac{\cos \theta_i - \sqrt{\frac{\epsilon_2}{\epsilon_1} - \sin^2 \theta_i}}{\cos \theta_i + \sqrt{\frac{\epsilon_2}{\epsilon_1} - \sin^2 \theta_i}} \quad , \tag{B.11}$$

and for vertical polarization

$$\frac{|E_r|}{|E_i|} = \frac{\frac{\epsilon_2}{\epsilon_1} \cos \theta_i - \sqrt{\frac{\epsilon_2}{\epsilon_1} - \sin^2 \theta_i}}{\frac{\epsilon_2}{\epsilon_1} \cos \theta_i + \sqrt{\frac{\epsilon_2}{\epsilon_1} - \sin^2 \theta_i}} \quad . \tag{B.12}$$

B.2 Development of Complex Permittivity

To accomodate the real earth ($\sigma > 0$), the *complex permittivitty* is developed. From Maxwell's equation as derived from Ampere's Law,

$$\nabla \times \mathbf{H} = (\sigma + j\omega\epsilon)\,\mathbf{E} \quad . \tag{B.13}$$

With a sinusoidal $\mathbf{E}$ represented by $E_o e^{j\omega t}$, let

$$\dot{\mathbf{E}} = j\omega E_o e^{j\omega t} = j\omega \mathbf{E} \quad , \tag{B.14}$$

leading to

$$\mathbf{E} = \frac{\dot{\mathbf{E}}}{j\omega} \quad . \tag{B.15}$$

B-3

Maxwell's equation is rewritten as

$$\nabla \times \mathbf{H} \;=\; \epsilon \dot{\mathbf{E}} + \sigma \mathbf{E} \tag{B.16}$$

$$=\; \epsilon \dot{\mathbf{E}} + \frac{\sigma}{j\omega} \dot{\mathbf{E}} \tag{B.17}$$

$$=\; \left(\epsilon + \frac{\sigma}{j\omega} \right) \dot{\mathbf{E}} \tag{B.18}$$

$$=\; \epsilon' \dot{\mathbf{E}} \tag{B.19}$$

with the complex permittivity ϵ'.

Using the complex permittivity, the new reflection coefficent for horizontal polarization becomes

$$R_h = \frac{|E_r|}{|E_i|} = \frac{\cos\theta_i - \sqrt{\left(\epsilon_r - j\frac{\sigma_1}{\omega\epsilon_o}\right) - \sin^2\theta_i}}{\cos\theta_i + \sqrt{\left(\epsilon_r - j\frac{\sigma_1}{\omega\epsilon_o}\right) - \sin^2\theta_i}} \quad , \tag{B.20}$$

and for vertical polarization

$$R_v = \frac{|E_r|}{|E_i|} = \frac{\left(\epsilon_r - j\frac{\sigma_1}{\omega\epsilon_o}\right)\cos\theta_i - \sqrt{\left(\epsilon_r - j\frac{\sigma_1}{\omega\epsilon_o}\right) - \sin^2\theta_i}}{\left(\epsilon_r - j\frac{\sigma_1}{\omega\epsilon_o}\right)\cos\theta_i + \sqrt{\left(\epsilon_r - j\frac{\sigma_1}{\omega\epsilon_o}\right) - \sin^2\theta_i}} \quad . \tag{B.21}$$

Appendix C. Numerical Electromagnetics Code Version 4.1

NEC4.1 is a Method of Moments code designed for wire and surface geometries in free-space, over a perfectly conducting ground plane and in the presence of a finitely conducting ground. This information is taken from Burke's manual (35:4–6,8–9).

C.1 The Electric Field Integral Equation (EFIE)

The NEC4.1 code is capable of using both the Electric Field Integral Equation (EFIE) and a Magnetic Field Integral Equation (MFIE). This research, though, only involves thin wires, so the only applicable equation is the EFIE. With the electric field of a volume current distribution, $\mathbf{J}$, the integral equation is

$$\mathbf{E}(\mathbf{r}) = \frac{-j\eta}{4\pi k} \int_V \mathbf{J}(\mathbf{r}') \cdot \bar{\bar{\mathbf{G}}}(\mathbf{r}, \mathbf{r}') \, dV' \quad, \tag{C.1}$$

where

$$\bar{\bar{\mathbf{G}}}(\mathbf{r}, \mathbf{r}') = \left(k^2 \bar{\bar{\mathbf{I}}} + \nabla\nabla\right) g(\mathbf{r}, \mathbf{r}') \quad, \tag{C.2}$$

$$g(\mathbf{r}, \mathbf{r}') = \frac{\exp\left(-jk|\mathbf{r} - \mathbf{r}'|\right)}{|\mathbf{r} - \mathbf{r}'|} \quad, \tag{C.3}$$

$$k = \omega\sqrt{\mu_o \epsilon_o} \quad, \tag{C.4}$$

and

$$\eta = \sqrt{\frac{\mu_o}{\epsilon_o}} \quad. \tag{C.5}$$

The time convention is $e^{j\omega t}$ and $\bar{\bar{\mathbf{I}}}$ is the identity diadic, $\hat{e}_x\hat{e}_x + \hat{e}_y\hat{e}_y + \hat{e}_z\hat{e}_z$. In the case where the current distribution is confined to the surface of a perfectly conducting body, the current density $\mathbf{J}$ becomes a surface current density, $\mathbf{J}_s$, and Equation C.1 becomes

$$\mathbf{E}(\mathbf{r}) = \frac{-j\eta}{4\pi k} \int_S \mathbf{J}_s(\mathbf{r}') \cdot \bar{\bar{\mathbf{G}}}(\mathbf{r}, \mathbf{r}') \, dA' \quad. \tag{C.6}$$

C-1

The code restricts the observation point **r** to be off the surface S, so that $\mathbf{r} \neq \mathbf{r}'$. Finally, the code approximates the surface current density, $\mathbf{J}_s$, of the wire as a uniform axial current, I, for a wire of radius a:

$$\mathbf{J}_s(\mathbf{r}) = \hat{\mathbf{s}} \frac{I(s)}{2\pi a} \quad , \tag{C.7}$$

where $\hat{\mathbf{s}}$ is the unit vector tangent to the wire axis and s is the distance along the wire.

C.2 The Moment Method Approach

The approach taken by NEC4.1 begins with the general equation for a linear operator,

$$Lf = e \quad , \tag{C.8}$$

where the linear operation is L (for this application the EFIE), f is an unknown response (the unknown currents), and e is a known excitation (corresponding to the gap voltage source used for this research). The unknown, f, is expanded in a sum of basis functions, f_j, as

$$f = \sum_{j=1}^{N} \alpha_j f_j \quad , \tag{C.9}$$

where α_j are unknown coefficients. Next, an inner product operator is defined as

$$\langle f, g \rangle = \int_S f(r) g(r) \, dA \quad . \tag{C.10}$$

To obtain a set of linear equations to solve for the coefficents, the inner product of Lf with a set of testing (or weighting) functions is performed and represented by

$$\langle w_i, Lf \rangle = \langle w_i, e \rangle \quad i = 1 \dots N \quad . \tag{C.11}$$

Since L is linear

$$\sum_{j=1}^{N} \alpha_j \langle w_i, Lf_j \rangle = \langle w_i, e \rangle \quad i = 1 \dots N \quad , \tag{C.12}$$

forming a set of linear equations written in matrix notation as

$$[G][A] = [E] \quad , \tag{C.13}$$

where $G_{ij} = \langle w_i, Lf_j \rangle$, $A_j = \alpha_j$, and $E_i = \langle w_i, e \rangle$. By inverting the G matrix, the solution for the currents is obtained as

$$[A] = [G]^{-1} [E] \quad . \tag{C.14}$$

The selection of basis and testing functions is critical to obtaining an accurate solution (35:9). For testing functions, w_i, NEC4.1 uses a point matching technique with impulse functions defined by

$$w_i(\mathbf{r}) = \delta(\mathbf{r} - \mathbf{r}_i) \quad . \tag{C.15}$$

The current basis functions for the wires take the form

$$I_j(s) = A_j + B_j \sin k_s(s - s_j) + C_j \left[\cos k_s(s - s_j) - 1 \right] \quad . \tag{C.16}$$

Bibliography

1. J.W. Rockway and J.C. Logan, *MININEC Broadcast Professional for Windows*, EM Scientific, Inc., 1996.

2. Douglas O. Reudink and M.F. Wazowicz, "Some Propagation Experiments Relating Foliage Loss and Diffraction Loss at X-band and UHF Frequencies", *IEEE Transactions on Communications*, vol. 21, no. 11, pp. 1198–1206, November 1973.

3. David E. Goldberg, *Genetic Algorithms in Search, Optimization, and Machine Learning*, Addison-Wesley Publishing Company, Inc., 1989.

4. Derek S. Linden and Edward E. Altshuler, "Automating Wire Antenna Design Using Genetic Algorithms", *Microwave Journal*, pp. 74–86, March 1996.

5. You-Cheol Jang, "Diffraction Analysis and Tactical Applications of Signal Propagation Over Rough Terrain", Master's thesis, Air Force Institute of Technology, 1997.

6. Merrill I. Skolnik, *Introduction to Radar Systems*, McGraw-Hill, Inc., second edition, 1980.

7. Tayeb A. Denidni and Gilles Y. Delisle, "A Nonlinear Algorithm for Output Power Maximization of an Indoor Adaptive Phased Array", *IEEE Transactions on Electromagnetic Compatibility*, vol. 37, no. 2, pp. 201–209, May 1995.

8. A. Sommerfeld, "Über die Ausbreitung der Wellen in der drahtlosen Telegraphie", *Annalen der Physik*, vol. 28, pp. 665–736, 1909.

9. K.A. Norton, "The Propagation of Radio Waves over the Surface of the Earth and in the Upper Atmosphere, Part I", *IRE Proceedings*, vol. 24, pp. 1367–1387, October 1936.

10. K.A. Norton, "The Physical Reality of Space and Surface Waves in the Radiation Field of Radio Antennas", *IRE Proceedings*, vol. 25, pp. 1192–1202, September 1937.

11. K.A. Norton, "The Propagation of Radio Waves over the Surface of the Earth and in the Upper Atmosphere, Part II", *IRE Proceedings*, vol. 25, pp. 1203–1236, September 1937.

12. Edward C. Jordan and Keith G. Balmain, *Electromagnetic Waves and Radiating Systems*, Prentice-Hall, Inc., second edition, 1968.

13. J.R. Wait, "Effect of the Ground Screen on the Field Radiated from a Monopole", *IEE Transactions on Antennas and Propagation*, vol. AP-4, no. 2, pp. 179–181, April 1956.

14. Robert E. Collin and Francis J. Zucker, *Antenna Theory, Part 2*, McGraw-Hill, Inc., 1969.

15. J.F. Ramsay, B.V. Popovich, and J.F. Gobler, "Research on Compact and Efficient Antennas", Tech. Rep. ECOM-02111-F, Airborne Instruments Laboratory, 1967.

16. Richard M. Thomas and Gregory R. Haack, "The Power Gain of a Vertical Monopole Antenna for Ground Wave Propagation", *Journal of Electrical and Electronics Engineering, Australia*, vol. 12, pp. 290–299, September 1992.

17. Valentin Trainotti, "MF AM Transmitting Asymmetric Vertical Dipole", *IEEE Transactions on Broadcasting*, vol. 37, no. 3, pp. 106–114, September 1991.

18. Ronold W.P. King and Sheldon S. Sandler, "The Electromagnetic Field of a Vertical Electric Dipole over the Earth or Sea", *IEEE Transactions on Antennas and Propagation*, vol. 42, pp. 382–389, March 1994.

19. Douglas M. Schwartz, "Antenna and Radiowave Propagation Characteristics at VHF Near and in the Ground", Master's thesis, University of Texas, 1963.

20. William Orr and Stuart Cowan, *Vertical Antennas*, Radio Publications, Inc., 1986.

21. Joseph J. Carr, *The Practical Antenna Handbook*, McGraw Hill, Inc., 1994.

22. Randy L. Haupt, "An Introduction to Genetic Algorithms for Electromagnetics", *IEEE Antennas and Propagation Magazine*, vol. 37, no. 2, pp. 7–15, April 1995.

23. M. Hindi and J.P. Daniel, "Synthesis of Slot Coupled Loaded Patch Antennas Using a Genetic Algorithm Through Various Examples", in *International Symposium 1997 Digest–Volume 3*. IEEE Antennas and Propagation Society, July 1997, pp. 1700–1703, IEEE Press.

24. Ahmad Cheldavi and Mahmoud Kamerei, "Practical Optimum Design for a Single-Layer Electromagnetic Wave Absorber at C and X-band Using Genetic Algorithm", in *International Symposium 1997 Digest–Volume 3*. IEEE Antennas and Propagation Society, July 1997, pp. 1708–1711, IEEE Press.

25. F. Ares, E. Villanueva, J.A. Rodriguez, and S.R. Rengarajan, "Application of Genetic Algorithms in the Design and Optimization of Array Patterns", in *International Symposium 1997 Digest–Volume 3*. IEEE Antennas and Propagation Society, July 1997, pp. 1684–1687, IEEE Press.

26. D.S. Weile and E. Michielssen, "Evolutionary Optimization of Electromagnetic Devices Using Advanced Operators and Population Structures", in *International Symposium 1997 Digest–Volume 3*. IEEE Antennas and Propagation Society, July 1997, pp. 1668–1671, IEEE Press.

27. Cinzia Zuffada, Tom Cwik, and Christopher Ditchman, "Synthesis of Novel All-Dielectric Grating Filters Using Genetic Algorithms", in *International Symposium 1997 Digest–Volume 3*. IEEE Antennas and Propagation Society, July 1997, pp. 1676–1679, IEEE Press.

28. Diogenes Marcano, "Synthesis of Linear and Planar Antenna Arrays Using Genetic Algorithms", in *International Symposium 1997 Digest–Volume 3*. IEEE Antennas and Propagation Society, July 1997, pp. 1688–1691, IEEE Press.

29. Raj Mittra, "Genetic Algorithm: The Last Word for Solving All of Your Design Problems?", in *International Symposium 1997 Digest–Volume 3*. IEEE Antennas and Propagation Society, July 1997, pp. 1672–1675, IEEE Press.

30. J. Michael Johnson and Yahya Rahmat-Samii, "Genetic Algorithms and Method of Moments (GA/MoM): A Novel Integration for Antenna Design", in *International Symposium 1997 Digest–Volume 3*. IEEE Antennas and Propagation Society, July 1997, pp. 1664–1667, IEEE Press.

31. Edward E. Altshuler, "A Monopole Antenna Loaded with a Modified Folded Dipole", *IEEE Transactions on Antennas and Propagation*, vol. 41, no. 7, pp. 871–876, July 1993.

32. Edward E. Altshuler and Derek S. Linden, "Design of a Loaded Monopole having Hemispherical Coverage Using a Genetic Algorithm", *IEEE Transactions on Antennas and Propagation*, vol. 45, pp. 1–4, January 1997.

33. Edward E. Altshuler and Derek S. Linden, "Design of a Vehicular Antenna for GPS/Iridium Using a Genetic Algorithm", in *International Symposium 1997 Digest–Volume 3*. IEEE Antennas and Propagation Society, July 1997, pp. 1680–1683, IEEE Press.

34. Derek S. Linden, "Using a Real Chromosome in a Genetic Algorithm for Wire Antenna Optimization", in *International Symposium 1997 Digest–Volume 3*. IEEE Antennas and Propagation Society, July 1997, pp. 1704–1707, IEEE Press.

35. Gerald J. Burke, *Numerical Electromagnetics Code–NEC-4, Method of Moments, Part II: Program Description–Theory*, Lawrence Livermore National Laboratory, 1992, UCRL-MA-109338 Pt. II.

36. Osama A. Mohammed, "GA Optimization in Electrical Devices", in *International Symposium 1997 Digest–Volume 3*. IEEE Antennas and Propagation Society, July 1997, pp. 1696–1699, IEEE Press.

37. Keen-Keong Yan and Yilong Lu, "Sidelobe Reduction in Array-Pattern Synthesis Using Genetic Algorithm", *IEEE Transactions on Antennas and Propagation*, vol. 45, no. 7, pp. 1117–1122, July 1997.

38. Charles E. Kaiser, "Refined Genetic Algorithms for Polypeptide Structure Predictions", Master's thesis, Air Force Institute of Technology, 1996.

39. Zebigniew Michalewicz and G. Nazhiyath, "GENOCOP III: A Co-Evolutionary Algorithm for Numerical Optimization Problems with Non-Linear Constraints", in *Proceedings of the Second IEEE International Conference on Evolutionary Computation*. 1995, pp. 647–651, IEEE Press.

40. Gerald J. Burke, *Numerical Electromagnetics Code–NEC-4, Method of Moments, Part I: Users Manual*, Lawrence Livermore National Laboratory, 1992, UCRL-MA-109338 Pt. I.

41. David A. Van Veldhuizen, Brian S. Sandlin, Robert E. Marmelstein, Gary B. Lamont, and Andrew J. Terzuoli, "Finding Improved Wire-Antenna Geometries with Genetic Algorithms", in *Proceedings of the 1998 International Conference on Evolutionary Computation*. IEEE Neural Networks Council and IEEE Alaska Session, 1998, pending acceptance.

42. Warren L. Stutzman and Gary A. Thiele, *Antenna Theory and Design*, John Wiley and Sons, Inc., 1981.

43. John D. Kraus, *Electromagnetics*, McGraw Hill, Inc., fourth edition, 1992.

44. Brian S. Sandlin and Andrew J. Terzuoli, "A Genetic Antenna Design for Improved Radiation over the Earth", in *Proceedings of the 1997 Antenna Applications Symposium*, 1997, pp. 301–314.

45. Constantine Balanis, *Antenna Theory, Analysis and Design*, John Wiley and Sons, Inc., second edition, 1997.

46. David E. Goldberg, Kalyanmoy Deb, and Bradley Korb, "Don't Worry, Be Messy", in *Proceedings of the Fourth International Conference on Genetic Algorithms*, Richard K. Belew and Lashon B. Booker, Eds. July 1991, pp. 24–30, Morgan Kaufmann Publishers, Inc.

47. Michael Barnsley, *Fractals Everywhere*, Academic Press, Inc., 1988.

48. Nathan Cohen, "Fractal Coding in Genetic Algorithm (GA) Antenna Optimization", in *International Symposium 1997 Digest–Volume 3*. IEEE Antennas and Propagation Society, July 1997, pp. 1692–1695, IEEE Press.

Vita

Brian Sandlin was born in the great Pacific Northwest, where his parents, Michael and Sheryl, and brother, Jason, continue to reside.

He received his Bachelor of Science in Electrical Engineering (BSEE) from the University of Portland in 1992, with an emphasis in computer engineering, particularly focusing on hardware and software development and microprocessor design.

Brian was commissioned into the Air Force in 1992 and entered active duty in 1993 to attend Undergraduate Space Training (UST) at the now defunct Lowry AFB, Colorado. Prior to AFIT, he was assigned to the 6th Space Operations Squadron (SOPS), Offutt Air Force Base (AFB), Nebraska, where he was a satellite operations flight commander and a satellite systems engineer for the Defense Meteorological Satellite Program (DMSP).

In Nebraska, Brian met Shonee Dale Bullin at one of his squadron's intramural football games in September of 1995. Nearly two years later Shonee became his wife, and they are the proud owners of two dogs, Jagger and Bailey, and the not-so-proud owners of one cat, Bootsie.

His follow on assignment is to the Radar Target Scatter (RATSCAT) Division of the 46th Test Group, Holloman AFB, New Mexico.

Permanent address: MP 0.65L Ausplund Road
                               Underwood, Washington

1. AGENCY USE ONLY *(Leave blank)*	2. REPORT DATE November 1997	3. REPORT TYPE AND DATES COVERED Master's Thesis

4. TITLE AND SUBTITLE
A WIRE ANTENNA DESIGNED FOR SPACE WAVE RADIATION OVER THE EARTH USING A GENETIC ALGORITHM

5. FUNDING NUMBERS

6. AUTHOR(S)
Brian S. Sandlin, Captain, USAF

7. PERFORMING ORGANIZATION NAME(S) AND ADDRESS(ES)
Air Force Institute of Technology
2750 P Street
WPAFB, OH 45433-7765

8. PERFORMING ORGANIZATION REPORT NUMBER

AFIT/GE/ENG/97D-10

9. SPONSORING/MONITORING AGENCY NAME(S) AND ADDRESS(ES)

10. SPONSORING/MONITORING AGENCY REPORT NUMBER

11. SUPPLEMENTARY NOTES

12a. DISTRIBUTION AVAILABILITY STATEMENT
Approved for public release; distribution unlimited

12b. DISTRIBUTION CODE

13. ABSTRACT *(Maximum 200 words)*
A wire antenna is designed for optimal performance at low elevation angles in the presence of a lossy half-space. A simple genetic algorithm (GA) and GENOCOP III software are each integrated with Numerical Electromagnetics Code Version 4.1 (NEC4.1) to optimize a wire antenna geometry for multiple objectives: power gain, azimuthal symmetry, and input impedance. The performance of the two versions of the integrated GA are compared. Several of the resulting antennas are analyzed, and an antenna is proposed for use in a Remote Intrusion Monitoring System (RIMS). Simulations suggest that the proposed antenna, which is well-matched, offers a significant increase in power gain at low elevation angles compared to the quarter-wavelength monopole. The performance of the proposed antenna surpasses that of the monopole at the necessary frequencies and a wide range of soil types. Also, the new antenna performance is not degraded by structure geometry perturbations.

14. SUBJECT TERMS
Antennas, Wire Antennas, Genetic Algorithms, Multi-Objective Optimization, Antenna Synthesis

15. NUMBER OF PAGES
114

16. PRICE CODE

17. SECURITY CLASSIFICATION OF REPORT	18. SECURITY CLASSIFICATION OF THIS PAGE	19. SECURITY CLASSIFICATION OF ABSTRACT	20. LIMITATION OF ABSTRACT
Unclassified	Unclassified	Unclassified	UL